UNIVERSITY OF OKLAHOMA

GRADUATE COLLEGE

ADDITIVE MANUFACTURING OF CONTINUOUS CARBON FIBER REINFORCED POLYLACTIC ACID COMPOSITES

A THESIS

SUBMITTED TO THE GRADUATE FACULTY

in partial fulfillment of the requirements for the

Degree of

MASTER OF SCIENCE

By

COLIN BRAY
Norman, Oklahoma
2020

ADDITIVE MANUFACTURING OF CONTINUOUS CARBON FIBER REINFORCED POLYLACTIC ACID COMPOSITES

A THESIS APPROVED FOR THE SCHOOL OF AEROSPACE AND MECHANICAL ENGINEERING

BY THE COMMITTEE CONSISTING OF

Dr. Yingtao Liu, Chair

Dr. Mrinal C. Saha, Co-Chair

Dr. M. Cengiz Altan

Acknowledgements

I would first like to thank God for the gifts that He has given me and for all the opportunities He has provided me in my academic career. I would like to thank Dr. Yingtao Liu of the University of Oklahoma for providing me the opportunity to pursue my master's degree in mechanical engineering by working in his lab. I would also like to thank Dr. Liu for his steadfast support, advice, guidance and mentorship of my graduate research. I truly appreciate the friendship that Dr. Liu and I have gained throughout my time working in his lab. I would like to thank Dr. Mrinal Saha for his commitment to the efforts of our lab as well. I, along with each other person in the lab, am very grateful for Dr. Saha's participation in our weekly meetings. I appreciate Dr. Saha's endless advice for my project; his numerous ideas were extremely helpful in the progression of my research. I would like to thank Dr. M. Cengiz Altan for his efforts in aiding my graduate studies and for providing me with a wealth of new knowledge on composite materials. I would like to thank Dr. Liu, Dr. Saha and Dr. Altan for their membership in my thesis committee.

I would not be where I am today without the people whom I have worked with both in the lab and throughout my coursework. I would like to thank my lab mates Blake Herren, Ben Hoelzel, Noah Golly, Weston Sleeper, Ryan Cowdrey, Dawaylon Barnes and George Huang for their friendship, camaraderie, and support throughout the past 2 years. I would also like to thank all the friends with whom I've taken courses during my time at OU who helped me to comprehend and master the material at hand. I would also like to thank Billy Mays, Greg Williams, Elijah Personette, Jonas Manchester and all of the other people who work in the machine shop; without your support in various aspects of my research, the success of my project would not be possible. Furthermore, I would like to thank all the AME staff members here at OU including Bethany

Burklund, Martina Ferguson, Ellen McKenzie, Melissa Foster and Rebeka Morales. Your guidance and assistance in various aspects of my project were imperative to its success.

I would like to particularly thank Anirban Mondal for your assistance throughout the last semester of this project. It was only through your dedication to this project that much of the data was acquired and many of the last samples were printed. I learned from you how to perform 3-point bending tests, take density measurements and calculate the fiber volume fraction of printed samples. The success of this project would not have been possible without your continued commitment.

Lastly, I would like to thank the people who I love and who I am closest to. I would like to thank my family, Dad, Mom, Caroline, Liam and Fiona, as well as Grandma, Grandpa, Pops, Ms. Carol and all of the other relatives for always being there for me and supporting me in whatever I do, including the pursuit of a master's degree. I would like to thank my incredible girlfriend Makenna for her endless support and enthusiasm in all that I do, including the pursuit of my master's degree. I would also like to thank my roommates Connor, Jake, Landon and Austin, as well as all of my rugby teammates and all of the other close friends that I have here at OU. Your support and friendship have been awesome throughout my academic career.

Dedication

I would like to dedicate this thesis to all the teachers, professors, coaches and mentors who I have had over the years who have shaped me into who I am today. It was only through their commitment to my future that I was able to grow and progress towards my goals.

Table of Contents

Table of Figures

Table of Tables

Abstract

Fused deposition modeling (FDM) is a category of additive manufacturing in which parts are fabricated via extrusion of material along a print path one layer at a time. A part is first created as a 3D computer-aided design (CAD) file before being converted to a standard tessellation language (STL) file, loaded into a slicer software such as Repetier-Host, and sliced. Slicing is the process of dividing the 3D digital model into layers for fabrication via additive manufacturing. G-code is generated as a result of this slicing process that dictates all necessary instructions to the printer for the fabrication of a part. In the case of this project, the g-code is then saved to a micro-USB drive before the drive is inserted into the printer.

Benefits of the fused deposition modeling process include great design freedom, cost-effectiveness, and versatility of materials and process. It is also well-known that adding reinforcement, such as continuous carbon fiber, to a thermoplastic matrix material can greatly increase material properties such as flexural strength. Thus, this thesis investigates the fabrication of continuous carbon fiber-reinforced polylactic acid (PLA) composites through in-nozzle impregnation. This involves feeding the fiber directly into the hot end of the printer prior to extrusion and extruding the continuous carbon fiber and PLA simultaneously through one nozzle. The continuous carbon fiber was coated prior to printing via a novel coating process that mitigated the issues of fiber fraying within the nozzle of the printer and tearing upon extrusion. Density and fiber volume fraction were measured in printed composites along with the completion of 3-point bending tests to measure flexural strength and elastic modulus. It was found that the addition of the continuous carbon fiber greatly increased both flexural strength and elastic modulus of printed samples when compared to samples printed of pure PLA. Furthermore, the effects of extrusion

temperature and layer height on impregnation of the fiber with PLA were characterized, and it was determined that a minimal layer height is optimal for fiber impregnation.

CHAPTER 1: INTRODUCTION

Section 1.1: State of the art of 3D printing composite materials

3D printing is a promising, relatively new field in which parts are manufactured in an additive process, contrary to more traditional subtractive manufacturing methods such as machining, milling or laser cutting. A part begins as a digital three-dimensional model constructed in a software such as Solidworks. The digital model is usually formatted as an STL (standard tessellation language) file. This file is then "sliced" in a slicer software, resulting in a new file consisting of two-dimensional layers that form the full three-dimensional part when the layers are oriented consecutively on top of each other.

The most common materials processed by 3D printing technology include thermoplastic polymers (such as ABS plastic, PLA plastic, polyamide and polycarbonate) and thermosetting polymer materials (such as epoxy resins) [1-4]. A major issue with the 3D printing of these common materials, however, is their lack of strength and functionality, particularly in load-bearing applications [5]. This is where 3D printing of polymer matrix composite materials becomes advantageous; combining matrix and reinforcement materials enables the 3D printing of a composite material that is either stronger or more functional (or both stronger and more functional) than the matrix materials or reinforcement materials would be alone [6]. Another advantage of 3D printing of polymers and composites is the ability to create complicated structures without the waste that is normal for traditional processes. 3D printing also allows for much more design freedom of internal structures, whereas fabrication of internal structures by traditional techniques is limited.

Composite materials have been 3D printed with several different types of reinforcement over recent years. These reinforcement materials can be classified as nanomaterials, particles, and

fibers [7-10]. The category of fiber reinforcements can be broken down into short fibers and continuous fibers. Furthermore, these different types of reinforcement materials have been 3D printed with matrix materials to form composites via several different printing techniques, including fused deposition modeling (FDM), powder bed and inkjet head 3D printing (3DP), stereolithography (SLA), selective laser sintering (SLS), 3D plotting and direct ink writing technology [11-16]. The employment of these techniques for the 3D printing of composite materials, along with the utilization of reinforcement material from one of the aforementioned categories, is discussed later in this chapter.

There have been multiple new techniques developed in recent years for the 3D printing of composite materials. A group published results in 2014 of Polyjet printing of shape memory polymer fibers printed in an elastomeric matrix to form origami [17]. Another group published results in 2015 of 3D printing silver nanoparticles and cross-linked polymer via digital light processing (DLP) for use as porous structures in applications such as 3D connectors for electrical circuits [18]. Yet another group published results in 2015 of 3D printing PLA and multi-walled carbon nanotube conductive microstructure composites via liquid deposition modeling (LDM) [19]. None of these newer composite 3D printing technologies are robust enough yet to become commercially viable, but all show promise.

3D printing of polymer composites has progressed greatly in recent years, yet this technology is still hindered by several limitations. The first of these limitations is the fact that there is only a small range of printable materials, and these materials usually do not meet the various requirements of a specific industry application [20]. The second of these limitations is that 3D printed polymer composites usually have lower mechanical strength and functionality than polymer composites fabricated by conventional molding methods. The third of these limitations is

the fact that the production capabilities of 3D printing machines are still well below the mark that they would need to reach to be industrially viable. 3D printing currently takes too long, cannot obtain very large part volumes, does not generally have feedback systems for errors, and often has significant room for improvement regarding part resolution [21]. Polymer composite 3D printing technology must progress past these limitations before it can be widely accepted in industrial applications.

Section 1.2: Nanomaterial-reinforced composites

Nanomaterials can act as valuable reinforcements to composites due to how they often have unique thermal, electrical and mechanical properties. Significant advancement of materials science has led to the rapid development of materials across multiple length scales and with numerous beneficial properties [22-28]. Nanomaterials that have been used in 3D printing processes include carbon nanotubes, graphene, graphite, ceramic, and metal nanoparticles [29-38]. It has been reported that the addition of carbon nanotubes to ethylene/1-octene copolymers both increased the thermal conductivity and affected the electrical conductivity of the resulting polymer nanocomposites [39]. It has also been reported that adding multi-walled carbon nanotubes to cyanate ester resin can enhance flexural strength and impact strength of the resin without sacrificing thermal stability [40]. It can be noted that in this case, the multi-walled carbon nanotubes were treated with pyrolysis and dense HNO_3/H_2SO_4 acids oxidation and that this treatment yielded regular arrangement and perfect crystal structure of the multi-walled carbon nanotubes.

Graphene has been reported to exhibit exceptional mechanical strength and thermal stability along with high electrical conductivity and biocompatibility, making it an excellent option as a reinforcement material in composites [41]. Results were published in 2015 of a study in which

graphite nanoplatelet/ultra-high molecular weight polyethylene nanocomposites were fabricated and exhibited a thermal conductivity coefficient that was 9 times higher than that of pure ultra-high molecular weight polyethylene matrix [42]. Another study, published in 2016, found that bismaleimide nanocomposites filled with polyhedral oligomeric silsesquioxane functionalized nanosized boron nitride exhibited a 266% increase in thermally conductive coefficient when compared to the bismaleimide matrix alone [43]. This is an example of how the incorporation of ceramic nanoparticles into composites can enhance material properties. Furthermore, a group published results of their research in 2014 in which 5 wt% nano-titanium dioxide (TiO_2) was added to acrylonitrile butadiene styrene (ABS) plastic. The group discovered a 13.2% increase in the ultimate tensile strength of the TiO_2/ABS composite material when compared to that of pure commercially available ABS plastic [44]. This is an example of how the incorporation of metal nanoparticles into polymer composites can enhance material properties.

One area in which nanomaterial-reinforced 3D printed composites have been successfully applied is the biomedical field. An example of this success can be found in the research of a group from Shanghai that was published in 2014. In their research, they manufactured magnetic Fe_3O_4 nanoparticles containing mesoporous bioactive glass/polycaprolactone (Fe_3O_4/MBG/PCL) composite scaffolds via the fused deposition modeling 3D printing technique [45]. These composite scaffolds were found to have a compressive strength of 13-16 MPa and excellent magnetic heating ability [45]. The scaffolds were also found to significantly stimulate proliferation, alkaline phosphatase activity, osteogenesis-related gene expression, and extra-cellular matrix mineralization of human bone marrow-derived mesenchymal stem cells [45]. The Fe_3O_4/MBG/PCL composites also showed the ability to release a drug over a sustained period of time, a capability that is applicable to local drug delivery therapy [45]. The group therefore

concluded that their nanomaterial-reinforced 3D printed composites exhibited the potential multifunctionality of local anticancer drug delivery, improved osteogenic activity and magnetic hyperthermia [45].

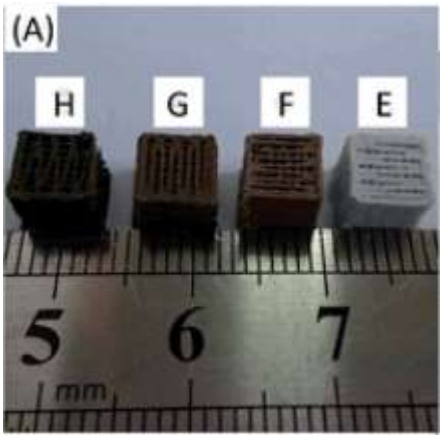

Figure 1: 3D Printed Fe_3O_4/MBG/PCL samples and MBG/PCL sample [45]

Figure 1 shows the various scaffold samples printed in the research mentioned above. Sample E is made of pure mesoporous bioactive glass/polycaprolactone, sample F is made of magnetic Fe_3O_4 nanoparticles containing mesoporous bioactive glass/polycaprolactone at 3.1 wt% Fe_3O_4, sample G is made of magnetic Fe_3O_4 nanoparticles containing mesoporous bioactive glass/polycaprolactone at 6.2 wt% Fe_3O_4, and sample H is made of magnetic Fe_3O_4 nanoparticles containing mesoporous bioactive glass/polycaprolactone at 9.3 wt% Fe_3O_4 [45].

Section 1.3: Particle-reinforced composites

Particles are also common reinforcement materials used in 3D printed composites. One advantage of particle reinforcements is their low cost. Another advantage is their capability to be easily mixed with polymers whether it be in powder form, liquid form or through extrusion into printable filament [1].

It has been reported that composites containing glass beads added to Nylon-11, fabricated via selective laser sintering, exhibit increasing tensile and compressive modulus while exhibiting decreasing strain at break and strain at yield as a function of glass bead volume fraction [46].

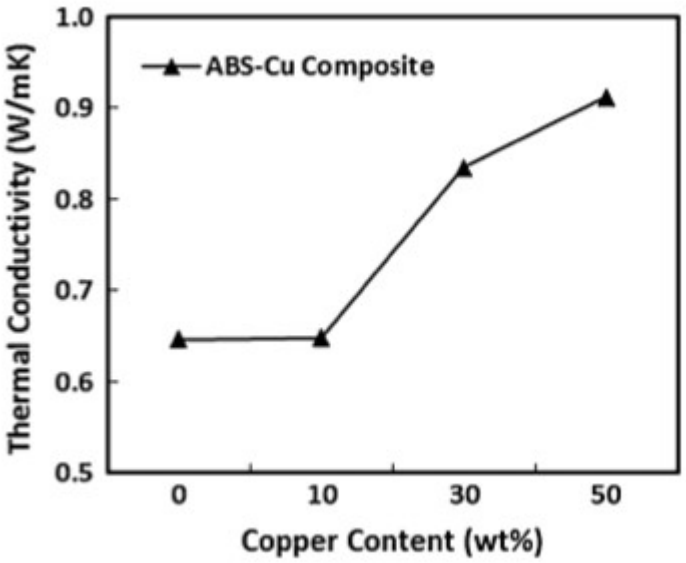

Figure 2: Thermal conductivity of ABS/Cu composite filaments [47]

It has also been reported, as seen in Figure 2 above, that composites containing iron and copper particles added to ABS plastic, fabricated via fused deposition modeling, exhibit improved thermal conductivity with increasing wt% of the metal [47]. This improved thermal conductivity could potentially enable the 3D printing of large-scale structures without the distortion that can come with thermal expansion of the polymer material.

An area in which particle-reinforced 3D printed composites have been successfully applied is the electronics field. Composite heat sinks and cooling coils, made of synthetic diamond microparticles and acrylate polymer, have been successfully fabricated via the stereolithographic technique for use as thermal management tools [48]. Applications of these tools include electronic and fluidic devices [48]. Two of the heat sinks printed are shown below in Figure 3.

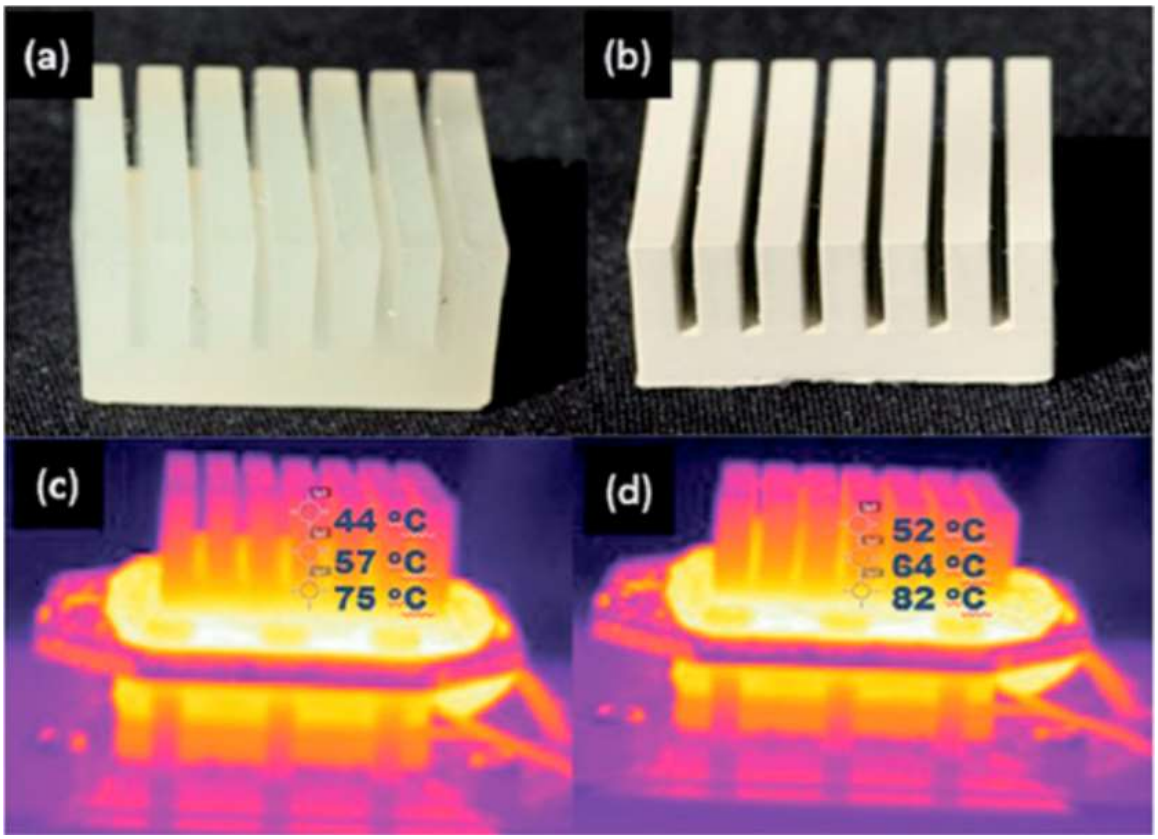

Figure 3: 3D printed heat sinks and their IR images when heated [1]

Image (a) of Figure 3 above shows a heat sink printed using pure acrylate polymer whereas image (b) of Figure 3 above shows a heat sink printed using 30% (w/v) acrylate polymer-diamond. Images (c) and (d) of Figure 3 above are IR images of the heat sinks when heated at 100 degrees Celsius for 10 minutes. One can note that for the 30% (w/v) acrylate polymer-diamond composite, the heat transfer rate exhibited significant improvement over the pure polymer material, as the acrylate polymer-diamond composite heat sink attains higher temperature values than the pure acrylate polymer heat sink when both are heated at the same temperature for the same time period [48].

Section 1.4: Short Fiber-Reinforced Composites

Multiple methods have been implemented in recent years to 3D print composites using short fibers as reinforcements, including the direct writing technique and fused deposition modeling. In one case, short glass fibers were prepared with ABS plastic, plasticizer and compatibilizer through extrusion to create a composite filament for 3D printing in the fused deposition modeling technique [49]. The incorporation of short glass fibers at 18 wt% increased the tensile strength of the material by 140% when compared to the observed tensile strength of pure ABS plastic. It can be noted that the addition of the short glass fibers reduced the flexibility and handleability of the material, thus rendering the need for plasticizer and compatibilizer. The inclusion of these two components improved the flexibility and handleability of the composite.

In another case, short carbon fibers were prepared with ABS plastic via extrusion into a composite filament [50]. The filament was then 3D printed via the fused deposition modeling technique into dog bone-shaped tensile samples. The tensile strength of the 40 wt% 3D printed short carbon fiber-ABS composite samples increased 115% from that of compression molded composites, whereas the modulus of the 3D printed samples increased 700% from that of compression molded composites. It can also be noted that the 3D printed composite samples were able to obtain a high fiber orientation in the printing direction (91.5% maximum) when compared to the compression molded composite samples.

Short carbon fiber-silicon carbide whisker-epoxy composites have been 3D printed via direct writing and have been found to exhibit a 127% improvement in tensile strength when compared to pure epoxy [51]. This was achieved by fabrication of an epoxy-based ink and control of the fiber and whisker reinforcement alignment.

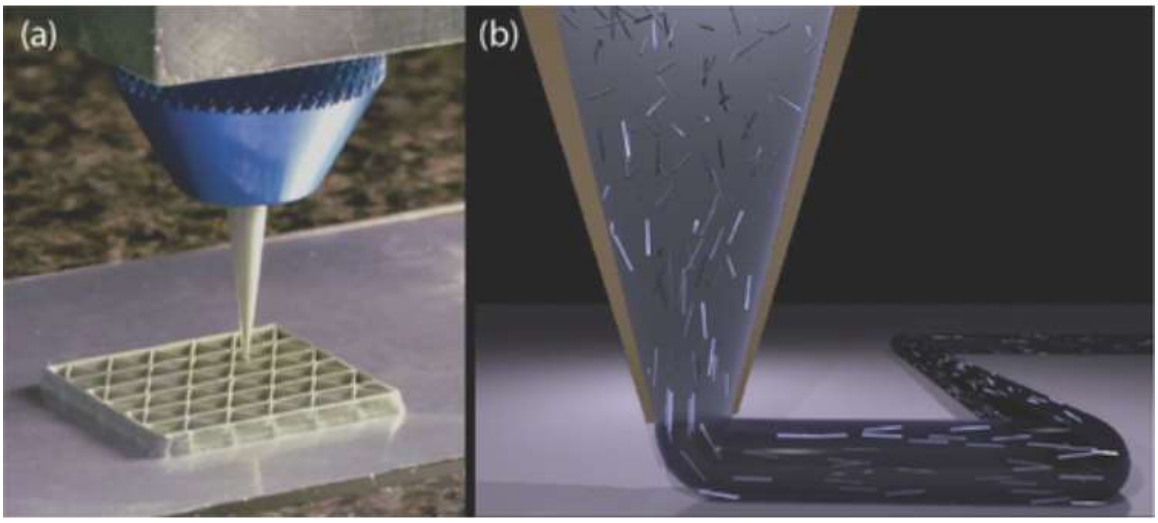

Figure 4: 3D printing of short fiber-reinforced composites [51]

Image (a) of Figure 4 above shows the 3D printing of a triangular honeycomb composite, whereas image (b) of Figure 4 above shows a schematic of the gradual alignment of high aspect ratio short carbon fibers and silicon carbide whiskers within the nozzle during the direct write process used to fabricate lightweight cellular composites [51]. It is this fiber and whisker alignment that enables the desired stiffness and toughness to be obtained in printed parts.

An area in which short fiber-reinforced 3D printed composites have been successfully applied is the biomedical field. Results have been published of 3D printed meniscus cartilage that was prepared by bioplotting and UV curing alginate/acrylamide gel precursor solution and an epoxy-based UV-curable adhesive [52]. Control of fiber distribution resulted in a range of swelling behavior in printed materials. Many soft tissues in the human body are similar in nature to fiber-reinforced hydrogel composites, therefore making this a potentially significant application for this type of 3D printed composite.

Section 1.5: Continuous Fiber-Reinforced Composites

The main technique that has been successfully implemented thus far in the 3D printing of continuous fiber-reinforced composites is fused deposition modeling. Within this technique, there have been several methods in which composite material has been printed. One of these methods utilizes 2 separate nozzles, one for extruding continuous fiber and one for extruding matrix material. This method was successfully implemented by a group who printed composite samples made of ABS plastic and either 1k continuous carbon fiber tow or glass fiber [53]. The bottom half of the samples would be printed with one nozzle and would be made entirely of ABS plastic, then the other nozzle would print several rows of fiber on top of the bottom half before the first nozzle would print the top half of the sample on the rows of fiber, sandwiching the fiber in the middle of the sample. The results of this study were a 17% gain in tensile strength and a 21% gain in Young's Modulus of the glass fiber-ABS plastic samples when compared to samples fabricated with pure ABS plastic. One can note that the fiber volume fraction of the composite glass fiber-ABS plastic samples was only 0.6%, obviously leaving much room for optimization through increasing the fiber volume fraction.

Another method for 3D printing with continuous carbon fiber involves preparing a filament with continuous fiber before feeding the filament into a fused deposition modeling 3D printer to be fabricated into parts. Results of one effort that employed this type of approach were published in 2018 in which 1k carbon fiber tow was coated with PLA plastic to create a prepreg filament before printing [54]. The apparatus used to prepare the continuous carbon fiber-PLA prepreg filament can be found below in Figure 5.

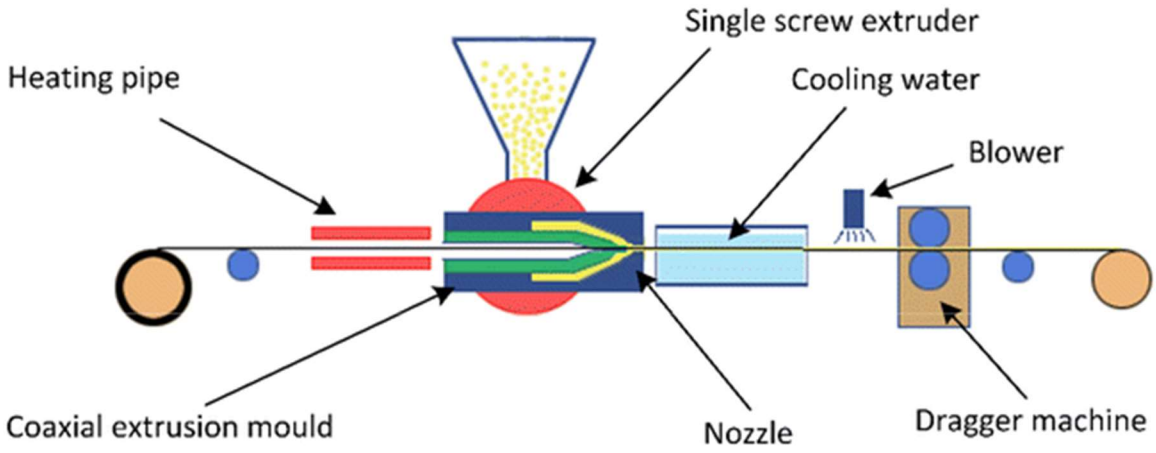

Figure 5: The filament preparation apparatus [54]

In Figure 5 above, one can observe that the carbon fiber tow is fed into a chamber along with PLA plastic pellets that are melted down before reaching the fiber [54]. The fiber is coated in the molten PLA plastic before a curing process that consists of drawing the coated fiber through cooling water and past a blower. Flexural samples were printed and exhibited more than double the flexural strength of samples prepared by the solution casting/hot press method. The samples also exhibited 61.7% better flexural strength than samples fabricated via the in-nozzle impregnation technique, described below.

The in-nozzle impregnation technique is the third method in which continuous carbon fiber-reinforced samples may be 3D printed. In this technique, matrix filament and carbon fiber are extruded out of one nozzle. Unlike when prepreg filament is used, however, the matrix filament and carbon fiber are fed into the nozzle separately and combine within the nozzle before extrusion. It has been reported that continuous carbon fiber-reinforced PLA plastic 3D printed samples fabricated via in-nozzle impregnation have exhibited a tensile modulus and tensile strength that are 599% and 435% of the tensile modulus and tensile strength of pure PLA plastic specimens [55]. This improvement in mechanical properties over pure PLA is much larger than the

improvement found in short fiber-reinforced PLA composites. This shows the promise of printing with continuous carbon fiber as a reinforcement material.

An area in which continuous fiber-reinforced 3D printed composites have been successfully applied is robotics. Markforged, a company that manufactures and sells 3D printers commercially, makes several printer models that print composites with continuous carbon fiber as a reinforcement. Haddington Dynamics, a company that manufactures robotic arms and kits, began 3D printing almost the entirety of its 7-axis robotic arms with carbon fiber-reinforced composite material, utilizing Markforged's printers to do so [56]. This transition saved Haddington Dynamics 58% in costs due to savings in volume.

Section 1.6: Comparison of Reinforcement Types

This section compares the 4 types of reinforcement that are used in the 3D printing of composites.

Table 1: Comparison of reinforcement type [1]

Reinforcement Type	Available Printing Techniques	Advantages	Disadvantages
Particle	• FDM • SLA • DLP • Selective Laser Sintering • Magnetically assisted DLP	• Low Cost • Easily mix with polymers	• Limited structural applications established thus far

	• Magnetically assisted direct writing		
Nanomaterial	• FDM • SLA • DLP • SLS • Solvent-cast direct writing	• Exhibit unique electrical, thermal and mechanical properties • Ability to create functionally graded composites	• Proper dispersion of nanomaterials in matrix can be challenging • Can potentially pose health risks
Short Fiber	• FDM • Direct write	• Can significantly improve structural properties while having capability of being printed via multiple techniques	• It is difficult to obtain a smooth layer of powder-fiber mixture in powder-based techniques • Maximum fiber content limited to 40 wt% due

			to nozzle clogging issues
Continuous Fiber	• FDM	• Often show the largest improvements in structural properties	• FDM is only technique that has consistently proven to be successful thus far

Table 1 above summarizes the 4 types of reinforcement used in 3D printed composite materials, listing the available printing techniques based on what has successfully been implemented thus far, advantages, and disadvantages for each reinforcement type. The reinforcement type used in this thesis is continuous fiber and the printing technique implemented is FDM. Continuous fiber was chosen due to how it often shows the largest improvements in structural properties and can be purchased relatively inexpensively. There are also several works currently available in which continuous fiber was employed in the FDM 3D printing technique; the availability of these works as reference material served as a great assistance in the progression of this project, providing further reason for choosing continuous carbon fiber as reinforcement material with FDM as the printing technique in this thesis. The fact that FDM is the only technique that has proven to be successful thus far in the 3D printing of continuous fiber composites is not a concern to this thesis, thus leaving no significant disadvantages for choosing continuous fiber reinforcement and the FDM printing technique for this thesis.

Section 1.7: Thesis Outline

The purpose of this thesis is to detail the progression of this project from design optimization of the printing process and apparatus through mechanical testing and characterization of 3D printed samples. Chapter 2 details the modification and optimization of the FDM printer used for this thesis including the mechanical design and electrical components of the final version of the printer. Chapter 3 details the fiber coating methodology implemented in this project including the parameters and process employed. Chapter 4 details the printing of samples for this project including sample modeling and G-code optimization, printing parameters, 3-point bending test sample details, laminates, line samples, and measurement and geometry shape validation. Chapter 5 details the mechanical testing of the 3D printed samples including density measurements, resin burn-off testing and fiber volume fraction measurements, and 3-point bending testing of 3D printed samples. Finally, Chapter 6 details the conclusions and future work of this project.

CHAPTER 2: FDM PRINTER MODIFICATION AND OPTIMIZATION

Section 2.1: Introduction

The additive manufacturing process utilized to 3D print with continuous carbon fiber in this project employs a fused deposition modeling, or FDM, printer. Specifically, a Creality CR-10 printer was commercially purchased for use in this project. This printer typically has the capability to 3D print parts with PLA plastic. After the modifications made in this project, however, the optimized Creality CR-10 printer can print PLA-continuous carbon fiber composites. This is done via the in-nozzle impregnation technique that was discussed in Section 1.5 above. Coated carbon fiber and PLA filament are both separately fed into the hot end of the printer and combine within the hot end's internal chamber. They are then both simultaneously extruded through a single nozzle to fabricate composite parts. This process is discussed in more detail in Section 2.2 below. The nozzle extrudes the composite PLA-carbon fiber material layer-by-layer to create parts. This process is controlled by g-code, which is later discussed in Section 4.1 and 4.2. The g-code dictates the nozzle's print path for one layer of the print, and when that layer is finished, the nozzle moves up in the z-direction and begins printing the next layer. Thus, the fabrication of parts via FDM is a layer-by-layer process. This is how composite parts were fabricated with the modified Creality CR-10 printer utilized in this project.

An image of the modified Creality CR-10 3D printer utilized in this project can be seen in Figure 6 below.

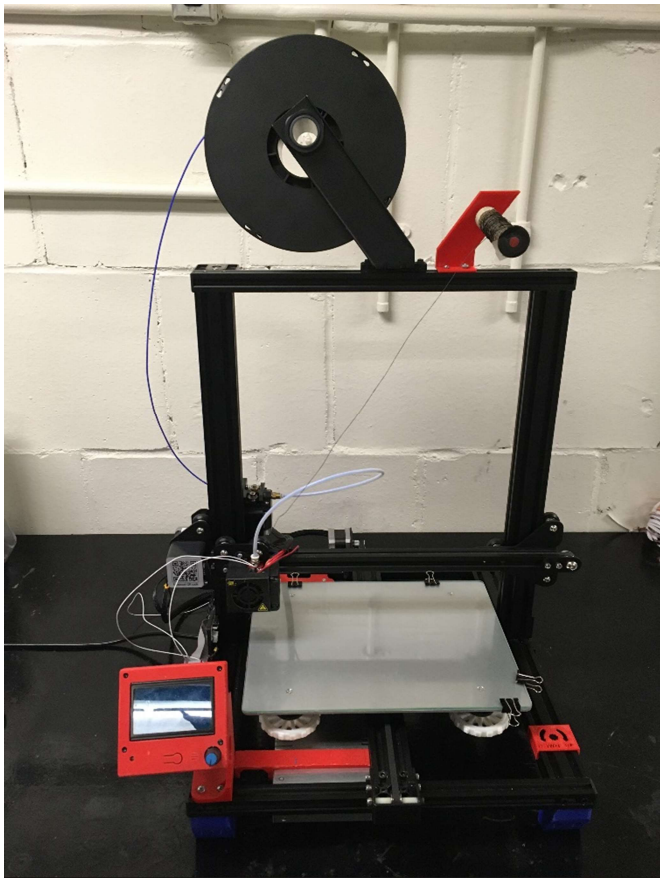

Figure 6: The printer used in this project

One can observe several of the modifications made to the Creality CR-10 3D printer utilized in this project in Figure 6 above. The most obvious modifications include the incorporation of a spool of carbon fiber that is mounted to the top of the 3D printer's frame and the strand of fiber that is fed into the hot end of the 3D printer. The following sections of this thesis detail the mechanical design and electrical components of this printer, including optimization of components belonging to each of these two categories. The main mechanical components of this printer include the stepper motors controlling the movement of the nozzle in each direction, the stepper motor controlling the extrusion of the PLA filament, the bed leveling mechanism, the parts included in the hot end, the cooling fans, the nozzle, the printer frame and the material used to adhere the prints to the printer bed. The main electrical components include the Ramps 1.4 electronics board, the

mosfet, the wiring configuration and the PID autotuning that was necessary in enabling proper heating of the hot end.

Section 2.2: Mechanical Design

The first step required in the assembly of this printer was the configuration of the printer frame. This frame is important because it ensures the stability of the entire printer. Thus, it must be made of a strong material. The frame of this printer is made of aluminum [57], providing the rigidity necessary to hold all printer components in place within a tight tolerance. The printer frame can be seen in Figure 6 above.

The next step required in the assembly of this printer was the installation and calibration of the stepper motors. The movement of the printer nozzle is controlled by 3 stepper motors: 1 in the x-direction, 1 in the y-direction and 1 in the z-direction. An image of one of these motors is shown below in Figure 7.

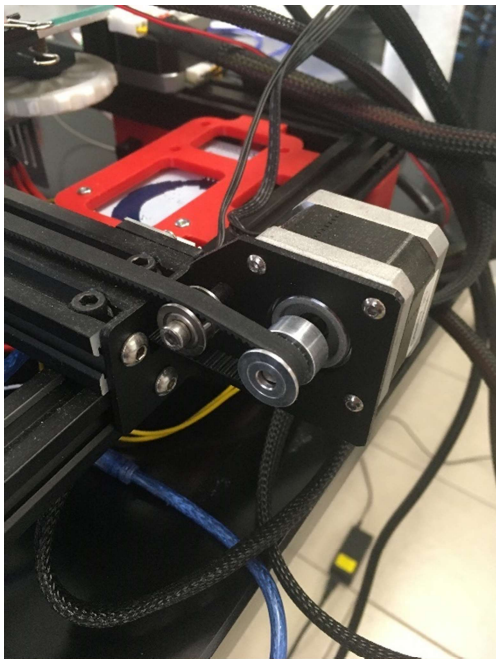

Figure 7: The y-direction stepper motor

As can be seen with the y-direction stepper motor in Figure 7 above, the x-direction and y-direction motors are each connected to a toothed wheel that is connected to a rubber belt. These belts are also connected to either the hot end (for movement in the x-direction) or the printer bed (for movement in the y-direction). The z-direction stepper motor is connected to a vertical threaded rod that rotates. This rod is connected to the crossbar that supports the hot end, and as the rod rotates, the hot end is either moved up or down. Furthermore, the extrusion of the PLA filament is controlled by a stepper motor. This motor turns a toothed wheel that pushes the PLA filament down the Bowden tube (the tube that feeds the filament into the printer's hot end). Therefore, the amount of PLA filament extruded per unit distance travelled is a direct function of the speed of the toothed wheel and thus this stepper motor. All stepper motors must be properly calibrated before the printer may be used. This is done by setting the "steps per millimeter" value for each motor. One step of a motor is equal to one tick of movement. To calibrate the steps per millimeter value of a stepper motor, the user must input a movement of a certain length to the motor and observe the actual distance travelled. If the two distances do not match, the user must adjust the steps per millimeter value accordingly. This is done for all stepper motors on the printer.

Leveling the printer bed is the next step in properly configuring the Creality CR-10 printer for the printing process. The bed must be level to ensure uniform layer height across the first layer of a print. Uniform layer height ensures optimal bed adhesion and print quality. If the layer height is too great, the extruded material will come out in chunks and will not fully adhere to the bed. This can lead to the print becoming warped and separated from the bed during a print. If the layer height is not great enough, the nozzle could compress the extruded material to the point of the fiber breaking. Even when printing without fiber, however, if the layer height is not great enough on any layer, large amounts of extruded material can be deposited on the side of the nozzle's path

during a print, leading to “ridges” between rows of print. To ensure that the first layer has uniform height and that none of these issues occur, the bed must be properly leveled before use of the printer. This is done by turning knobs underneath the print bed. An image of one of these knobs can be seen in Figure 8 below.

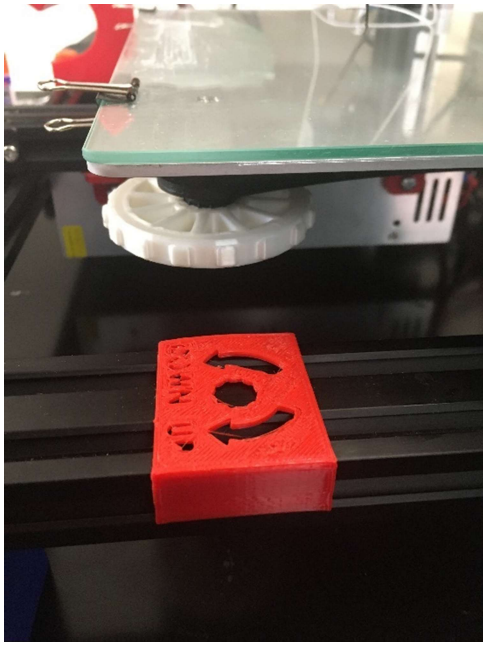

Figure 8: A bed-leveling knob

In Figure 8 above, the white part in the shape of a wheel is the bed-leveling knob for the front-right corner of the print bed. The actual knob itself is small and in the center of the white wheel; the white wheel is a 3D printed attachment to make the knob easier to turn. One can also note the red 3D printed sign mounted on the printer frame. This sign shows how turning the white knob clockwise moves the print bed up and turning the knob counterclockwise moves the print bed down. There are 4 knobs in total, with one knob at each corner of the print bed. Turning a knob either raises or lowers the bed at that corner. Prior to the initial use of the printer used for this project, the bed was properly leveled using these knobs.

Perhaps the most critical group of components in the mechanical design of this printer includes the components that comprise the hot end. This includes the heating block, the heat sink, the nozzle, and the carbon fiber feed pipe. The PLA filament is initially housed on a spool that is mounted on top of the printer. This is shown below in Figure 9, where one can observe the blue PLA filament coming off of the mounted circular spool.

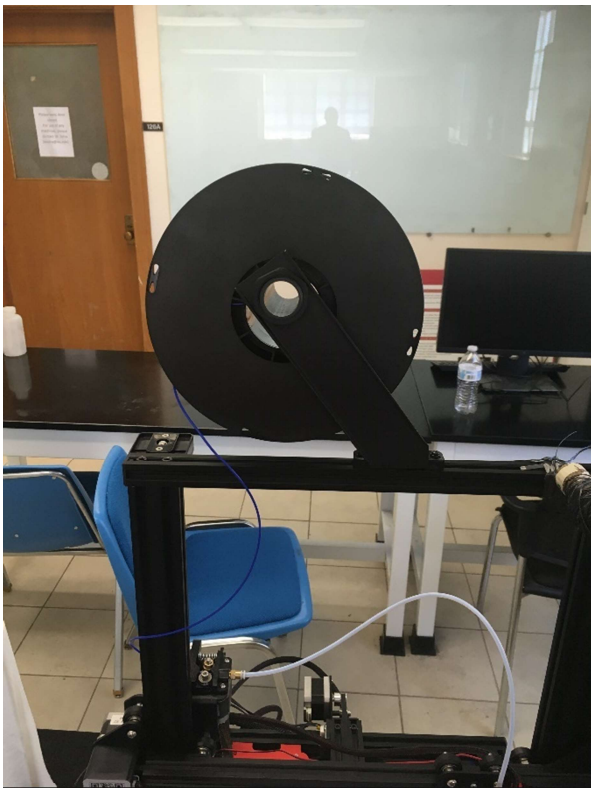

Figure 9: The mounted PLA spool

The filament is pulled from the spool by the extruder stepper motor and subsequently pushed through a tube known as a Bowden tube, pictured in Figure 10 below.

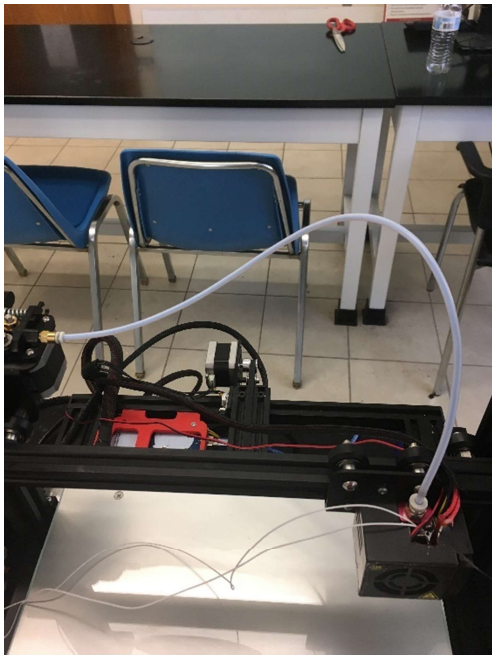

Figure 10: The Bowden tube

In Figure 10 above, the Bowden tube is the white tube that runs form the extruder stepper motor to the top of the hot end. This tube is screwed in at both locations to secure the connection while also allowing for easy removal. The hot end apparatus is shown below in Figure 11.

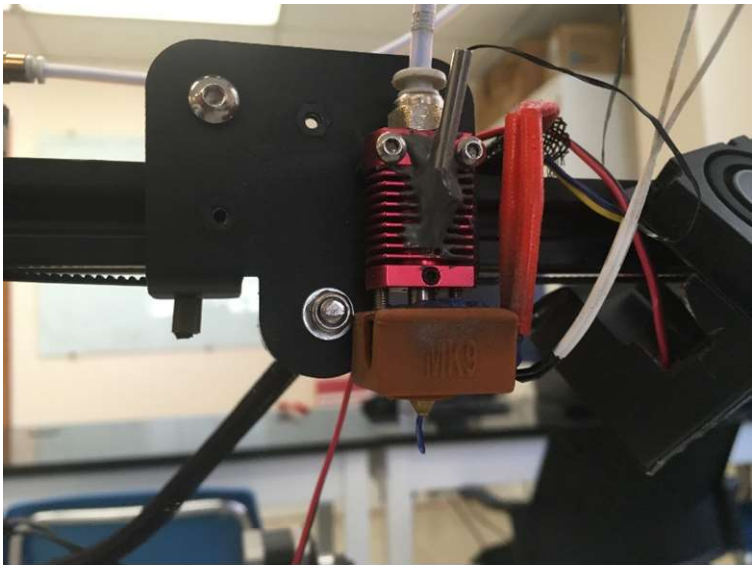

Figure 11: The hot end apparatus

In Figure 11 above, the red component is the heat sink. The metal pipe that protrudes from the heat sink is the carbon feed pipe. The orange component below the heat sink, in the shape of a rectangular prism, is the heating block. One can observe that two black and white wires, as well as two red cables, are connected to the heating block. The black and white wires connect the thermistor to the electronics board for temperature control. This is discussed in greater detail in Section 2.3 below. The red cables connect the heating block to the power supply and are the means by which the heating block is heated. One can also note that the heating block is actually inside of the orange material visible in Figure 11 above; the orange material is a thin silicone sleeve that fits over the heating block. This sleeve is necessary because it insulates the heating block from the air blowing on it from the cooling fans, enabling the heating block to reach the set temperature. The component below the heating block is the nozzle. A Solidworks model of this modified hot end apparatus is shown below in Figure 12.

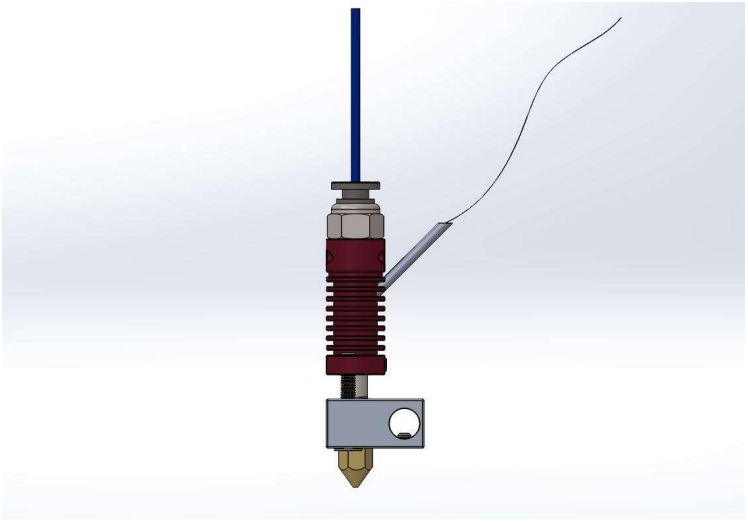

Figure 12: A Solidworks model of the hot end apparatus

The heating block reaches a temperature of 230 degrees Celsius during prints, and thus the heat sink is necessary to dissipate this heat from the hot end before it reaches the Bowden tube. Aiding in the dissipation of this heat is a cooling fan, shown below in Figure 13.

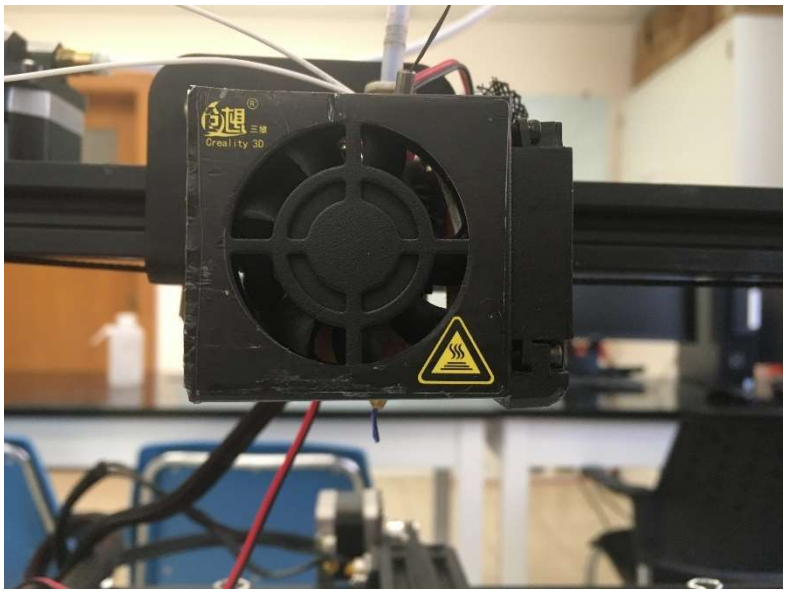

Figure 13: The hot end cooling fan

The fan in Figure 13 blows on the hot end apparatus. This helps to ensure that the PLA filament remains cool and therefore in a solid state before it reaches the heating block. If the PLA filament heats up before the heating block, it can become molten inside of the heat sink and then re-solidify, causing clogging. So, the PLA filament is pushed from the Bowden tube down through the heat sink and into the heating block. The heating block, as previously mentioned, is heated to a temperature of 230 degrees Celsius during prints, and this temperature is enough to melt the PLA plastic before it is pushed from the heating block and through the nozzle for extrusion. Before the PLA filament even reaches the heating block, however, it is joined by the carbon fiber tow. This was made possible by first drilling an angled hole through the heat sink to the chamber inside the heat sink that guides the PLA filament through. A small hollow cylindrical metal pipe was then pressed into the hole and bound in place by J-B Weld. An image of this pipe is shown in the blue box in Figure 14 below.

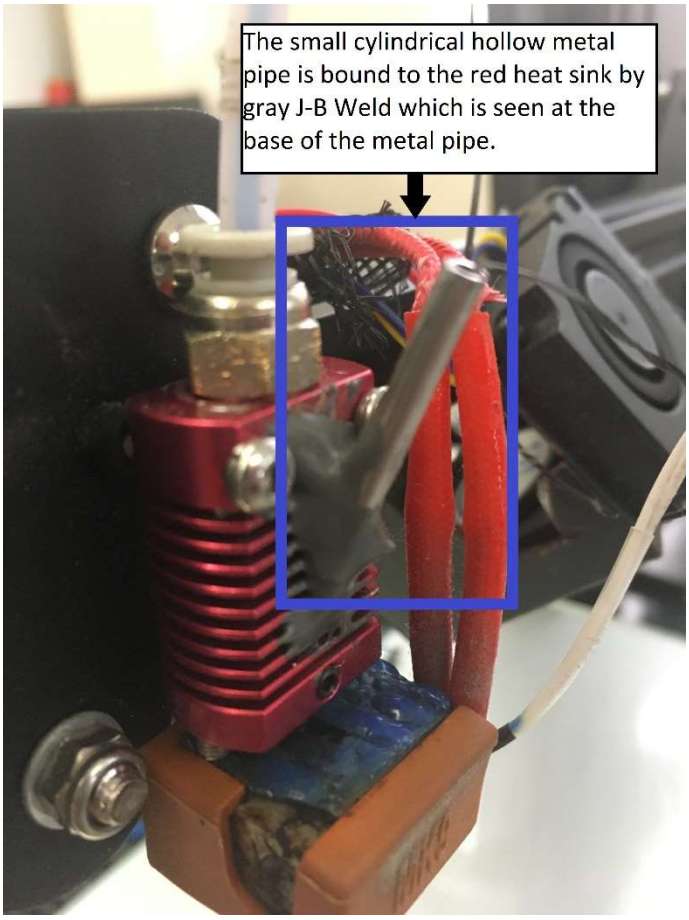

Figure 14: The carbon fiber feed pipe

One can see in Figure 14 above how the metal feed pipe is connected to the red heat sink at an angle and bound to the heat sink by J-B Weld; the J-B Weld is the dark gray material that surrounds the connection between the feed pipe and the heat sink. The carbon fiber tow is initially housed on a spool that is mounted on top of the printer, similar to the PLA filament. This spool is shown in Figure 15 below.

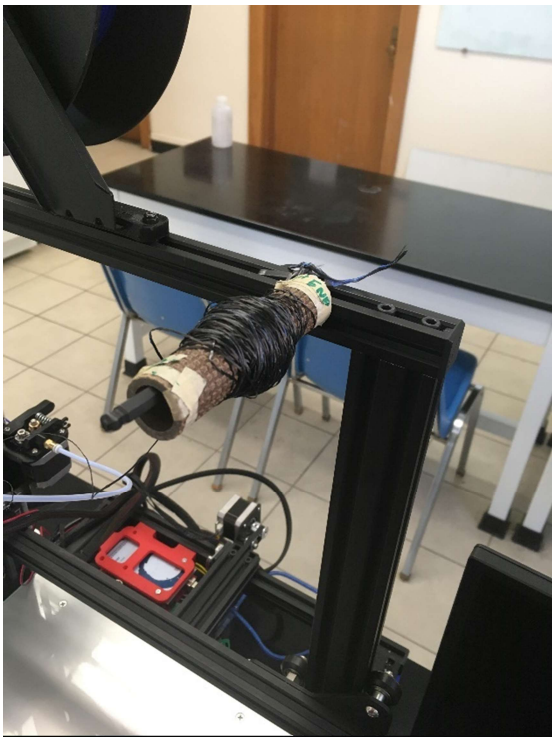

Figure 15: The mounted carbon fiber spool

The fiber is fed from the spool shown in Figure 15 above down through the small hollow cylindrical metal pipe into the heat sink, where it then joins with the PLA filament while the PLA filament is still in its solid state. When the fiber and PLA filament reach the heating block, the PLA melts and impregnates the fiber within the hot end apparatus prior to extrusion. The PLA-carbon fiber composite material is then extruded through a single nozzle. There is no pushing or pulling mechanism necessary to feed the carbon fiber through this process, as it is pulled through by the tension applied to it by the already-printed material that has solidified. The solidification of the material that has been extruded by the nozzle is aided by the use of a cooling fan. This fan is shown in Figure 16 below.

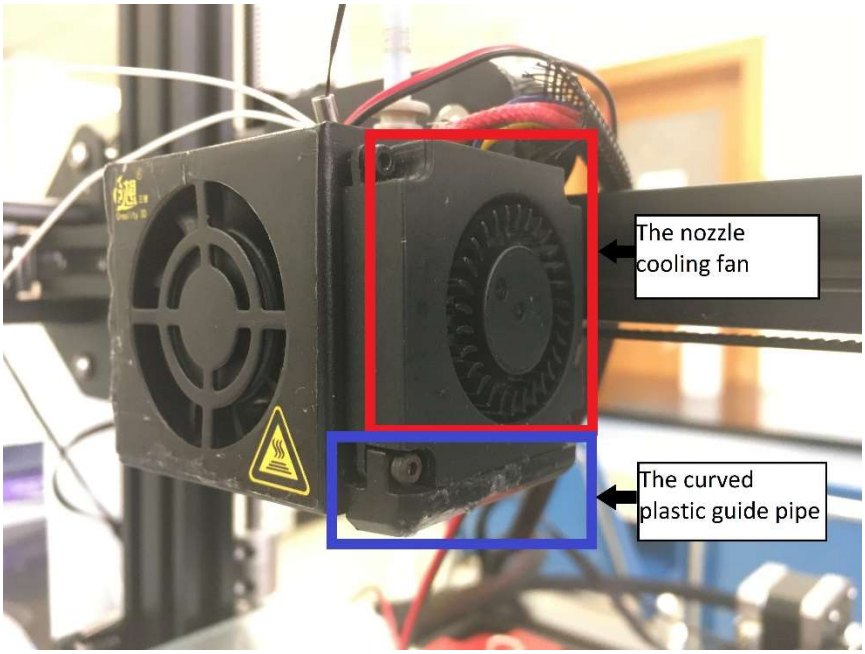

Figure 16: The nozzle cooling fan

In Figure 16 above, the nozzle cooling fan is located on the side of the hot end cooling fan and is found within the red box. There is a curved plastic guide pipe that directs the air from this fan towards the bottom of the nozzle; this guide pipe is found within the blue box in Figure 16. The guide pipe helps to cool and consequently solidify the printed material more quickly.

It can be noted that the nozzle itself was also modified for this project. The most common inner diameter dimension for a nozzle of an FDM printer such as the Creality CR-10 is 0.4 mm. The nozzle used in this printing process, however, has an inner diameter of 1.5 mm. This was accomplished by drilling a 1.5 mm-diameter hole at the opening of a 0.4 mm-diameter nozzle. The difference in nozzle inner diameter dimension between a typical 0.4 mm-diameter nozzle and the 1.5 mm-diameter nozzle used for this project can be observed in Figure 17 below. In the figure, the top 2 images are the engineering drawings for each nozzle inner diameter size, whereas the bottom image is a picture of both nozzles.

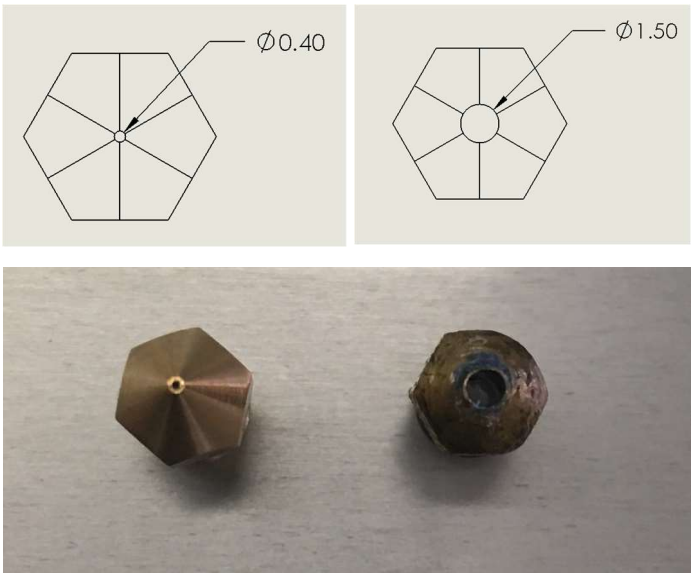

Figure 17: 0.4mm and 1.5mm diameter nozzles

One of the most critical parts of a successful print in this project has been proper bed adhesion. Any print that does not adhere properly to the bed is subject to becoming disconnected from the bed, which can cause warping of the part. The bed of the Creality CR-10 printer consists of a glass plate that is laid on top of a metal plate. Printing directly on the glass without modification is not sufficient for proper bed adhesion. When printing pure PLA plastic parts, a layer of blue painter's tape is commonly applied to the glass print bed to provide adequate bed adhesion. Blue painter's tape, however, does not provide enough bed adhesion for composite PLA/continuous carbon fiber prints. Therefore, a layer of Elmer's Disappearing Purple glue stick is applied directly to the glass print bed in this process. One can note that, due to the slow print speed being utilized, the glue is reapplied to the bed multiple times throughout the printing of the first layer of a sample. This ensures that the glue has not fully dried when the nozzle reaches any particular point in the print path of the first layer. An image of the print bed with Elmer's Disappearing Purple glue stick applied can be seen in Figure 18 below.

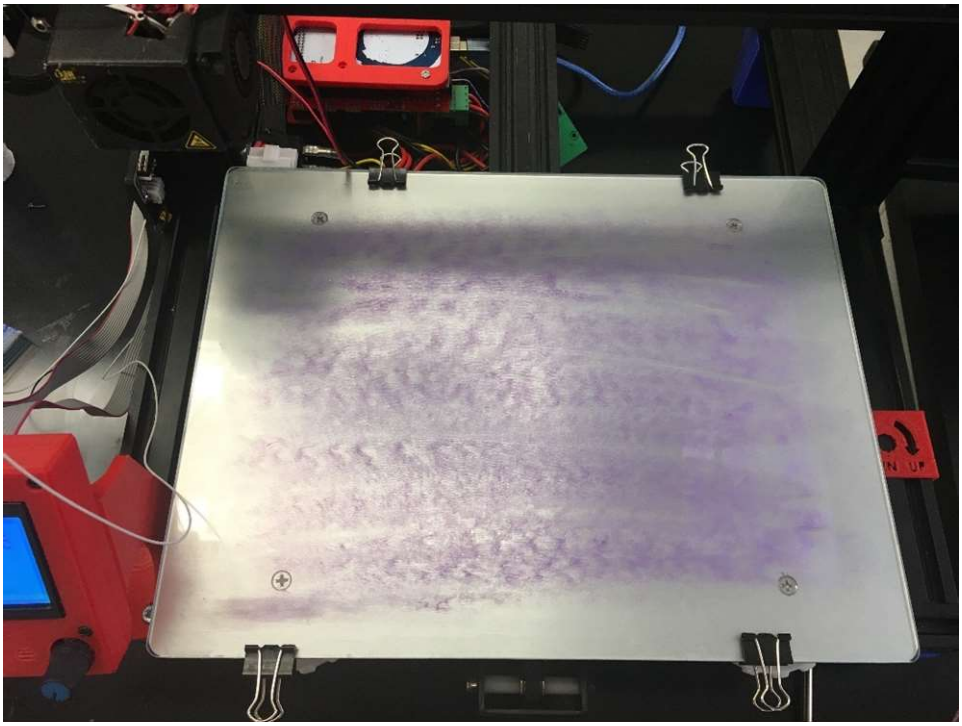

Figure 18: The print bed with glue stick applied

One issue with using a highly adhesive material such as glue stick is that prints are more difficult to remove from the print bed at the conclusion of printing. This has not been an issue for prints that are 3 or more layers thick. For single layer prints, however, issues with removing the print from the print bed have been encountered due to an overly strong bond between the print and the print bed. Specifically, the prints would fracture along the edges between print paths. To counter this issue, a layer of release film was glued onto the print bed for single layer prints. A layer of Elmer's Disappearing Purple glue stick was then applied on top of the release film, and the print was conducted on this layer of glue. At the conclusion of the print, the release film was peeled off the glass print bed, thus peeling the print with it. The release film was then peeled off the print. This process enabled the fabrication of single layer prints without any issues involving the removal of the prints from the bed. An image of the print bed with release film and glue stick applied can be seen in Figure 19 below.

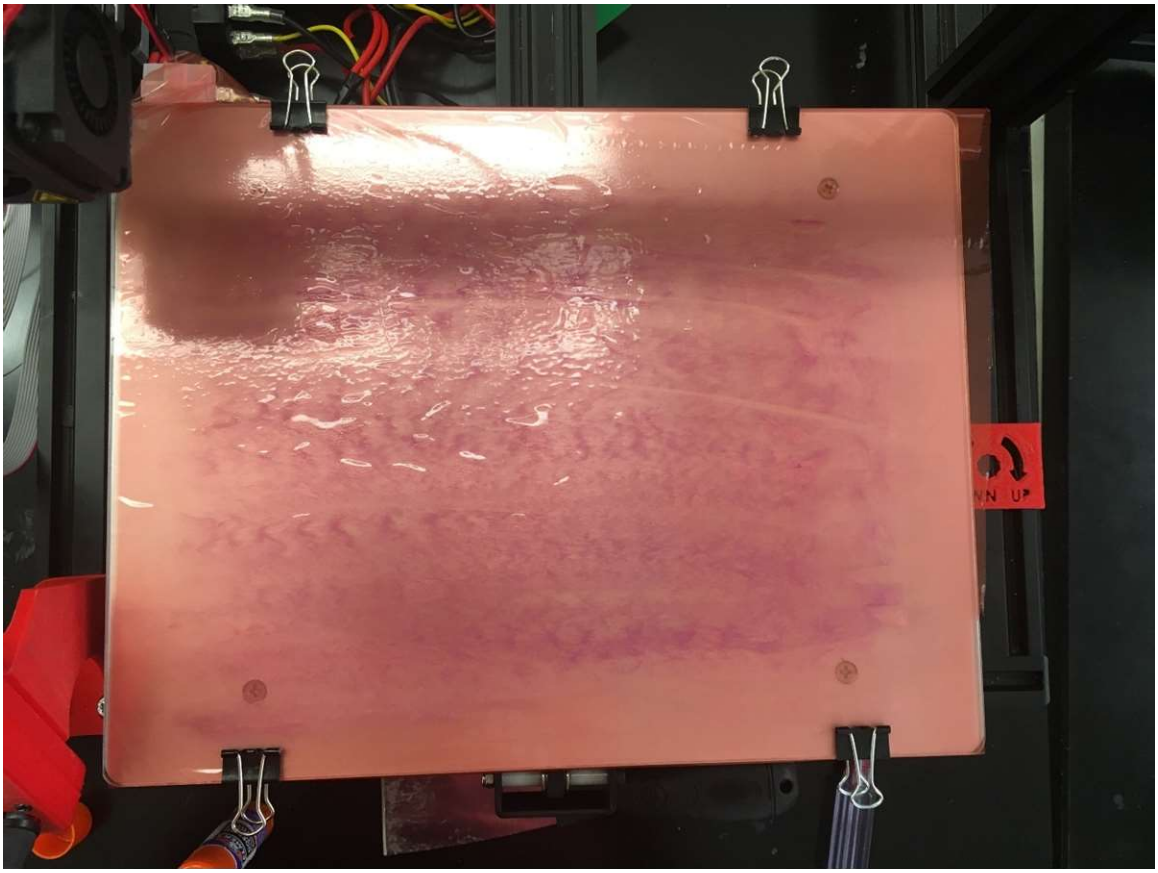

Figure 19: The print bed with release film and glue stick applied

Whether the release film was utilized or only glue stick was utilized, the samples had to be cleaned off after the printing process to remove any excess adhesive material. This was done by wetting a paper towel with water and wiping the samples off with the wet paper towel before subsequently drying them off with a dry paper towel.

The final component of the printer's mechanical design is the heated bed. It was discovered through experimentation that the composite prints of this research adhere to the bed best when the bed is not heated. Although the bed is not heated during the finalized printing process, the bed has the capability to heat up to improve bed adhesion in certain cases and several previous iterations of the printing process detailed in this paper incorporated the heated bed. The bed can reliably heat

up to at least 80 degrees Celsius. The heated bed, particularly its electrical components, is explored in more detail in Section 2.3 below.

Section 2.3: Electrical Components

There are several main electrical components to the printer used in this project. These include the power supply, the Ramps 1.4 board, the Arduino Mega 2560 board, the mosfet, and the LCD screen. The printer is plugged into a typical wall outlet, and the power from this outlet is wired into the power supply. The input of power to the power supply from the wall outlet is controlled by a switch, which either turns the printer on or off when flipped. The power supply used for the printer in this project is the same as the one shown in Figure 20 below.

Figure 20: The power supply [58]

One can note that the power supply has an output voltage of DC 12V, 360W, 30A and an input voltage of AC 100-120V, 60Hz [58]. Thus, the power supply acts as a transformer as it converts the power from AC to DC. The power supply is made out of stainless steel, which

provides added protection and durability [58]. One can observe the connectors on the left side of the power supply in Figure 20; these connectors are where the wires that connect the power supply to the rest of the electrical components of the printer are attached. There are 3 connectors for positive DC output, 3 connectors for negative DC output, and 3 connectors for AC input. The power supply outputs power to either the Ramps 1.4 board or to the mosfet, both of which are discussed below.

The Ramps 1.4 board works in conjunction with the Arduino Mega 2560 board to control all electronics of the printer. These two boards are pictured below in Figure 21.

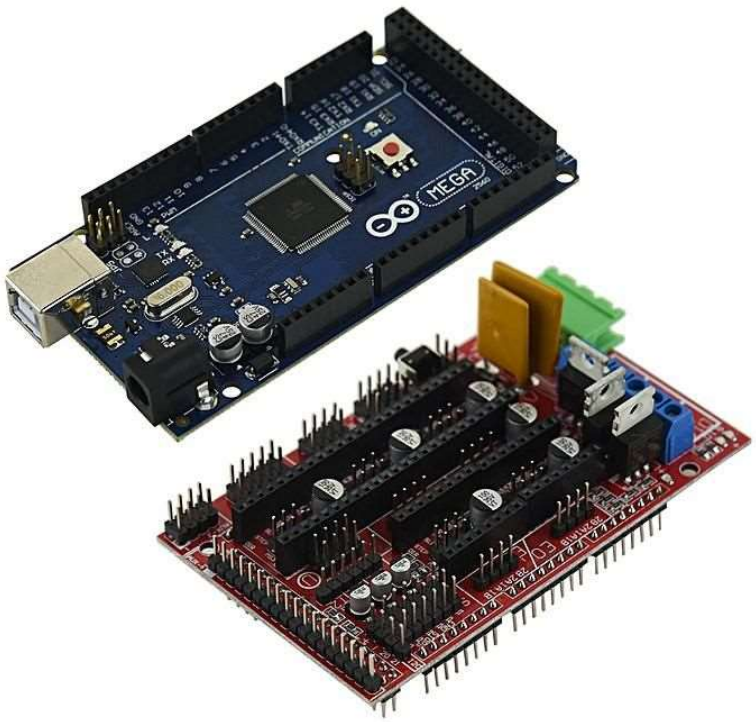

Figure 21: The Arduino Mega 2560 and Ramps 1.4 boards [59]

The blue board in Figure 21 above is the Arduino Mega 2560 board, whereas the red board pictured above is the Ramps 1.4 board. The Arduino Mega 2560 board functions as a microcontroller that stores the printer's firmware, which is the primary code that dictates the

function of each component of the printer. The firmware for this printer was configured through an open source software before being stored in the Arduino Mega 2560 board. The Ramps 1.4 board electrically controls each individual component of the printer based on the firmware stored in the Arduino Meg 2560 board. This is accomplished by sending the correct amount of current and voltage to the appropriate port during the printer's operation. This process is all dictated by the g-code generated for each print. The g-code is discussed in greater detail in Section 4.1.

Another significant electronic component of this printer, although not necessary in the final printing process that was used to fabricate the samples reported on in this thesis, is the Mosfet.

Figure 22: A Creality CR-10 Mosfet [60]

Figure 22 above shows a Mosfet of the same variety that was used with the printer used in this project. The Mosfet enables proper heating of the heated bed, which is the reason for why it is not necessary in the final printing process used to fabricate samples in this project since the heated bed was not utilized in this process. Nevertheless, the heated bed was utilized in many of the trials leading up to the finalization of the printing process, and thus the Mosfet was still a

critical component in this project's iterative approach. The heated bed did not receive the required voltage from the Ramps 1.4 board alone to heat up to the temperature set in the g-code. Thus, voltage was input to the Mosfet from both the power supply and the Ramps 1.4 board, along with control input from the Ramps 1.4 board. When the Ramps 1.4 board sent the control signal to the Mosfet to heat the printer bed, the Mosfet would take the input voltage from both the power supply and Ramps 1.4 board and output the voltage to the printer bed. The printer bed therefore received a greater amount of voltage than it had been receiving from the Ramps 1.4 board alone. This enabled the printer bed to successfully heat to whatever temperature was set every time.

The LCD screen is yet another critical component of the printer's operation. The screen is pictured below in Figure 23.

Figure 23: The LCD screen [61]

The LCD screen connects to the Ramps 1.4 board and allows the user to directly control all functions of the printer. This includes heating the hot end and/or the print bed, jogging any of the stepper motors, setting the fan speed for the hot end cooling fans, and running any of the saved

g-code to produce a print. The g-code is saved on a micro-SD card that is inserted into a slot in the LCD screen. Without the LCD screen, the user would only be able to control printer function through connecting a computer to the Ramps 1.4 board.

One issue encountered during this process was that the hot end was initially unable to heat up to 230 degrees Celsius when both cooling fans were at full speed. This is an issue because if the hot end is heated to such a high temperature when the cooling fans are at reduced speeds, the heat sink is not adequately cooled and the PLA within the heat sink may consequently become molten. This can lead to solidification of the PLA within the heat sink and therefore clogging of the inner chamber of the heat sink. There were three measures implemented to counter this issue. First, a silicone sleeve was fitted around the outside of the heating block to help insulate it from the cool air being blown from the cooling fans. This sleeve is shown in Figure 12 and was previously discussed in Section 2.2. Secondly, the thermistor cables that feed into the heating block were replaced. These cables can also be seen in Figure 12.

The third measure implemented was performing a PID autotune. PID stands for "proportional integral derivative" and a PID autotune in the case of the printer in this project is essentially an adjustment of parameters to control the temperature of the nozzle. After a successful PID autotune, a 3D printer nozzle should be able to maintain a set temperature within a small tolerance. In the case of this printer, that means reaching the 230 degrees Celsius mark necessary for printing the samples in this project. This is not the first time PID autotuning has been used to improve a nozzle's accuracy in maintaining a set temperature in a 3D printing process. Work was published in 2017 in which PID autotuning was used to improve the nozzle heating accuracy in a 3D printer that used an Arduino Mega 2560 board and a Ramps 1.4 board [62], just like the printer in this project. It was reported that after taking 115 seconds to run the autotune, the printer could

maintain a temperature with a steady state error of only 1% of the set temperature [62]. This supports the effectiveness of a PID autotune in improving a 3D printer's ability to maintain a set temperature within a small error. The open source software Repetier-Host was used to perform a PID autotune in this project. This is done by opening Repetier-Host on a laptop and connecting the laptop to the Ramps 1.4 board. Through Repetier-Host, the user can input commands to the printer to control any function that can be controlled directly through the LCD screen, including additional functions. Once the laptop is connected to the Ramps 1.4 board and the Repetier-Host software is open, the user inputs the commands M303 E0 S230. This tells the printer to heat the first nozzle and cycle around a temperature of 230 degrees Celsius to find the correct values of P, I and D. 230 degrees Celsius was chosen because this is the temperature at which the prints are fabricated. One must note that it is important that the nozzle is at room temperature and that the fans are on full speed before the start of the PID autotune. After performing an autotune, values of P = 12.14, I = 0.47 and D = 77.79 were reported. These values were then input into the printer's firmware, and the firmware was saved with the new values. This process, along with replacing the thermistor cables and fitting a silicone cover over the heating block, enabled the nozzle of the printer in this project to consistently reach 230 degrees Celsius while the cooling fans are blowing at full speed.

CHAPTER 3: FIBER COATING METHODOLOGY

Section 3.1: Introduction

A critical step in this printing process is the coating of the carbon fiber tow prior to printing. Initially, the carbon fiber tow was left uncoated as it was fed into the hot end of the printer. This caused a couple of issues that prevented successful prints from being completed. The main issue caused by utilizing uncoated fiber tow was that the tow would fray inside the hot end prior to extrusion, as there was nothing to keep the individual fibers of the tow bound together. Over time, the frayed material would build up in the nozzle, and eventually the nozzle would clog. This would always occur long before even a single layer of a sample could be completed. Another issue that would occur when utilizing uncoated fiber tow was that the fiber could more easily tear upon extrusion from the nozzle during the printing process when compared to coated carbon fiber tow. This is likely due to the fact that the coating on the coated tow protects the fibers as the tow moves across the bottom edge of the nozzle during extrusion. The uncoated carbon fiber tow doesn't have this protection, and since the bottom edge of the nozzle comes to a relatively thin edge, the uncoated carbon fiber tow can easily be torn by this edge upon extrusion.

These are the main reasons for why it is highly beneficial to coat the carbon fiber tow used in this process. Once the tow was coated, it no longer frayed in the hot end and only tore upon extrusion on rare occasions.

Section 3.2: Fiber Coating Parameters and Process

This is not the first time that continuous fiber has been coated before utilization in an additive manufacturing process. Work was published in 2016 in which continuous carbon fiber 1k tow was coated in a solution of PLA plastic, methylene dichloride, and deionized water [11]. The PLA particles were added to the methylene dichloride solution at 8% mass fraction, magnetically

stirred for 30 minutes, sheared and emulsified before deionized water was added to the solution [11]. The 1k continuous carbon fiber tow was then submerged in the solution to complete the coating process [11]. This is similar to the coating process employed in this project, although there are some notable differences. First and foremost, the materials used to coat fiber in this project are chloroform and scrap PLA plastic. Chloroform was chosen because it has the ability to dissolve PLA. Roughly 2 fluid ounces of chloroform are poured into a small 4-ounce jar and massed. The PLA plastic is taken from the filament that typically feeds into the 3D printer used in this project. The filament is cut into very small pieces using a pair of scissors and is then massed so that the mass of the PLA plastic is 9.55% mass fraction of the final mixture of PLA and chloroform. This mass fraction was chosen because the PLA mass fraction used in the paper mentioned above was 8%. 9.55% is a value that is very close to 8%, but slightly higher to promote more viscosity in the solution and thus greater retention of PLA on the carbon fibers after coating. This helps to ensure that no fraying takes place in the hot end during printing, as discussed above. Once the PLA has been cut and massed, it is added to the chloroform in the 4-ounce jar. A magnetic stir bar is also added to the jar, and the jar is then placed on a magnetic stir plate and magnetically stirred at 750 rpm for 5 hours. By the end of this 5-hour period, the pieces of PLA have broken down and the mixture has become a viscous solution. At this point, the jar is removed from the magnetic stir plate, and the lid of the jar is taken off and replaced with a modified lid. This lid is pictured below in Figure 24.

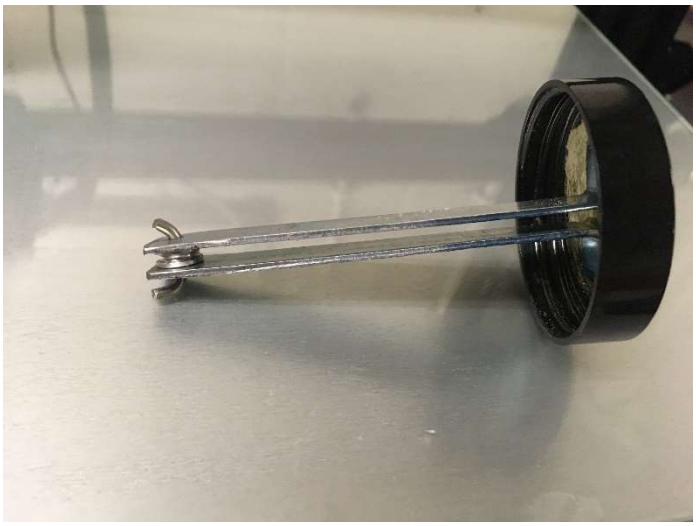

Figure 24: The modified lid

As one can observe in Figure 24 above, the modified lid consists of a wheel mounted onto the bottom of two metal bars protruding from the bottom of the lid. There are two holes drilled into the lid, one larger and one smaller. The smaller hole has a diameter of 0.03 mm, which is only slightly larger than the diameter of the coated fiber. The larger hole has a diameter of 0.10 mm. An image of the jar with the modified lid attached is shown below in Figure 25.

Figure 25: The modified lid screwed onto a jar

The fiber is fed through the larger hole in the modified lid, wraps around the wheel at the bottom of the two metal bars, and is pulled back out of the jar through the smaller hole. The wheel is low enough in the jar that it is fully submerged in the PLA/chloroform solution, ensuring that the fiber gets thoroughly coated. One can also note that there is a groove in the center of the wheel which ensures that the fiber does not slip off of the wheel during the coating process. The fact that the diameter of the smaller hole is only slightly larger than the diameter of the coated fiber means that any excess PLA/chloroform solution stuck to the fiber prior to passing through the smaller hole will be scraped off the fiber as the fiber is pulled through the smaller hole and thus out of the jar. This is important, as any excess PLA that dries on the fiber after coating can potentially get caught in the carbon fiber feed pipe as the fiber is fed into the hot end during the printing process, thus tearing the fiber. Once the fiber has been fed through the modified jar, it is dried with a heat

gun before being wound back on a spool. A schematic of this entire process is shown below in Figure 26.

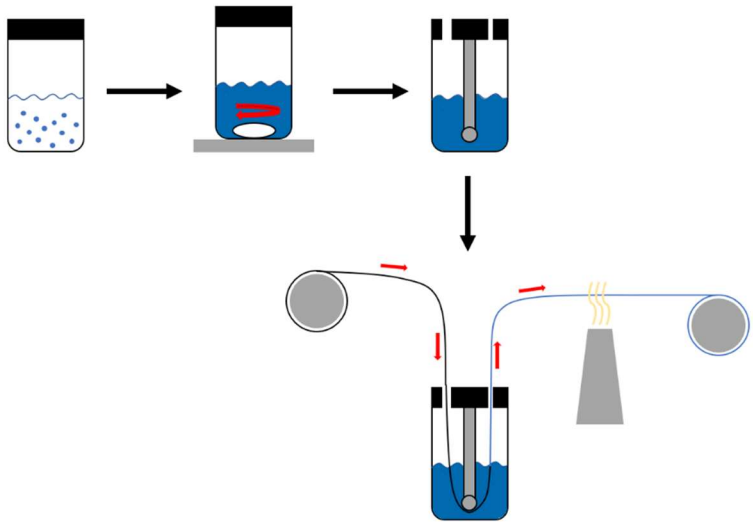

Figure 26: The fiber coating process

The heat gun in the above process helps to ensure that the coating is dried on the fiber before being wound back on the new spool. If the fiber isn't dried, the fiber may become stuck to itself when it is wound around the spool, which can lead to tearing. Once the fiber has been wound onto the new spool, it is ready to be utilized in the printing process.

CHAPTER 4: PRINTING OF SAMPLES

Section 4.1: Sample Modeling and G-Code Optimization

The 3D digital models for the samples printed in this project were all first created in Solidworks. Solidworks is a computer-aided design and computer-aided engineering software that enables a user to efficiently produce 3D digital models. The models produced in this project include 3-point bending test models, small 1, 3- and 5-layer laminate models, large 5-layer laminate models and line sample models. The 3-point bending test models were fabricated according to ASTM standard D790. According to this standard, samples must have a rectangular cross-section and a span-to-depth ratio of 16:1 unless a larger span-to-depth ratio is necessary. The standard states that for high-strength reinforced composites, a span-to-depth ratio of 32:1 or 40:1 is recommended. The samples produced in this project are high-strength reinforced composites and therefore have a span-to-depth ratio of approximately 50:1, with dimensions of 122.564 mm in length, 15.950 mm in width and 1.800 mm in thickness. The span-to-depth ratio is smaller than the total length-to-thickness ratio, as the span-to-depth ratio takes the distance between the two mounts in the 3-point bending test as the span of the specimen. This is discussed in greater detail in Section 4.6 below. Images of the 3D digital models of these samples in Solidworks can be found in Figure 27 below.

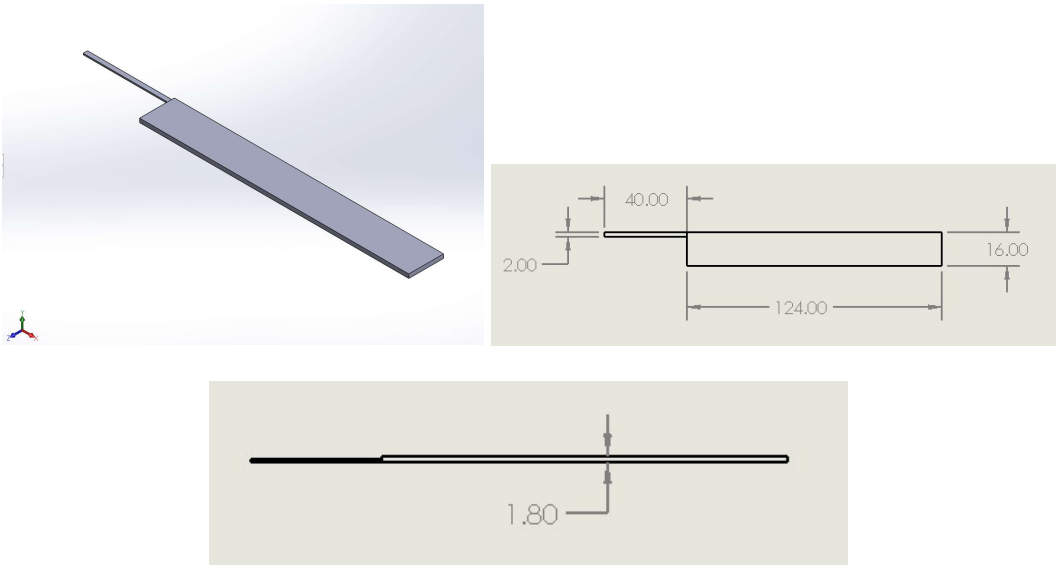

Figure 27: The 3-point bending samples

One can note that the dimensions for length and width in the digital models are slightly larger than the dimensions for length and width once the models have been sliced (and subsequently printed). This is because the slicer must keep the dimensions in increments of the extrusion width and the actual printed samples are not exactly equal to the set dimensions. One can also note the narrow, single-layer extension protruding from the corner of the sample. This was where the print started; it takes a few moments for the material to extrude evenly when a print begins, and thus this extension allows time for the extrusion to even out before the actual sample gets underway. When the sample is finished printing, the extension is cut off. After the models shown in Figure 27 above were created, they were saved as STL files. The STL file is the typical file type used in 3D printing. STL files only account for the surface geometry of 3D objects and approximate this geometry with an array of triangles. Once the models were saved in the STL file format, they were loaded into Repetier-Host. At this point, the models were sliced with the printing parameters described in Section 4.2 below. Slicing is the process of dividing a model up into layers prior to the printing process. In the fused deposition modeling form of 3D printing, 3D objects are

fabricated layer-by-layer from the bottom to the top. Slicing prepares the g-code that dictates this layer-by-layer process. The g-code controls the printer's movement by giving absolute coordinates in the x- and y-directions for each of the nozzle's print paths along with an extrusion amount for each path. The print paths for one layer are all completed before the print paths for the next layer are started, hence the layer-by-layer approach. The sliced 3-point bending test models are shown below in Figure 28.

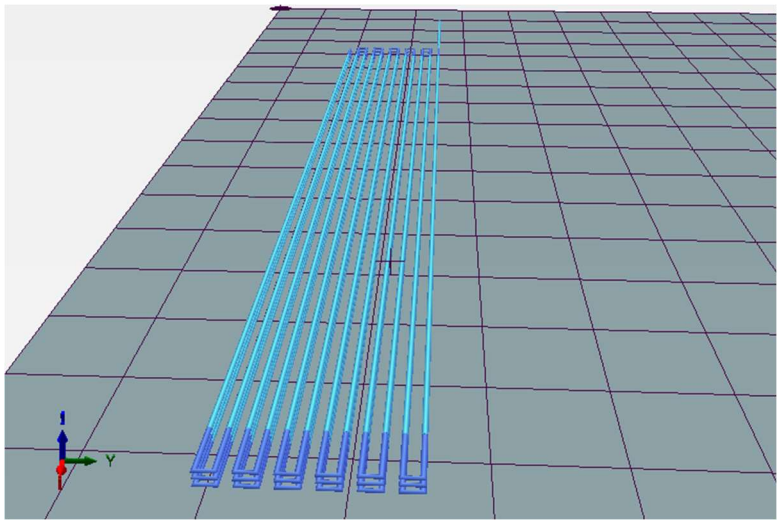

Figure 28: Sliced 3-point bending test model

In Figure 28 above, the dark blue sections are where the nozzle moves at 1 mm/s whereas the light blue sections are where the nozzle moves at 2 mm/s. One can also observe how the models are sliced layer-by-layer, with an aligned rectilinear print path. This print path is shown below in Figure 29.

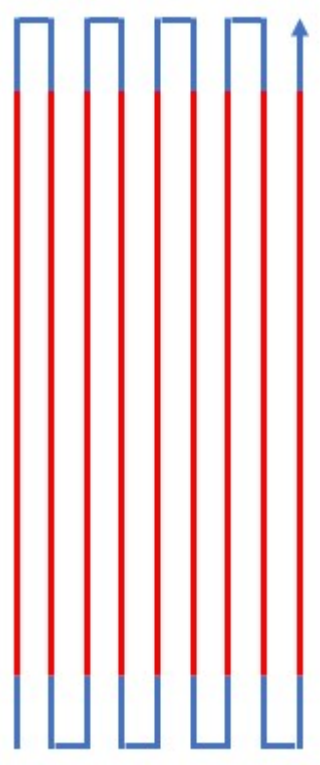

Figure 29: The print path for 3-point bending samples

In Figure 29 above, the blue sections of the print path have print speeds of 1 mm/s, whereas the red sections of the print path have print speeds of 2 mm/s. This is done because the nozzle cannot move faster than 1 mm/s around the corners or else the fiber will tear. Along the straightaways, however, the nozzle can move 2 mm/s without the fiber tearing. Thus, the print time of samples is minimized when the print speed is 2 mm/s everywhere except around the corners. One can also note that the print path of a layer starts where the print path of the previous layer ends. Thus, there are no "travel moves" anywhere during a print. A travel move is when the nozzle moves but does not extrude any material; this is typically utilized to print different sections of a layer that are not connected. When printing with continuous fiber, however, travel moves cannot be utilized, as the fiber would continue to extrude out of the nozzle and pull molten PLA with it should a travel move be attempted. This would be an issue as the material extruded during the

travel move would block later print paths in the print. The main parameters that were set for the 3-point bending samples are discussed in Section 4.2 below. Once these parameters were set and the models were sliced, however, the g-code was generated and ready to be saved onto an SD card. From there, the SD card was taken out of the computer and inserted into the LCD screen of the printer, and the samples were printed. The printing process is described in Section 4.3 below.

Both the pure PLA 3-point bending test samples and the continuous 1k carbon fiber tow 3-point bending test samples were fabricated in the exact same way, using all the same steps listed above. Both types of samples had the same print paths and print speeds, were the same size, and used the same printing parameters that are described in Section 4.2 below. The carbon fiber simply wasn't fed into the hot end during fabrication of the pure PLA 3-point bending test samples. The same amount of PLA was extruded per unit length, however, in the pure PLA samples as was extruded per unit length in the continuous 1k carbon fiber reinforced samples.

Later in the project, 3-point bending test samples were fabricated with 3k continuous carbon fiber. These samples were sliced differently than the other 3-point bending test samples. This is due to the fact that, because of the 3k tow's larger size, more PLA must be pushed out of the nozzle along with it in order to ensure enough PLA is extruded. With the same slicing and printing parameters as the 1k carbon fiber reinforced samples, the 3k carbon fiber reinforced samples would have gaps between rows of print due to under-extrusion of the PLA. More about the printing parameters of the 3k carbon fiber reinforced small laminates is discussed in Section 4.2 below. Furthermore, although the print path is still the same as that of the other 3-point bending test samples (as seen in Figure 29), the gaps between rows of print are smaller and the layer height is larger for the 3k carbon fiber reinforced 3-point bending test samples. The print speed is maintained at 1 mm/s throughout the entire print, as this is an easier speed to print at and thus a

safer option to utilize, as 3k fiber is more difficult to print with than 1k fiber. An image of a sliced 3k continuous carbon fiber reinforced 3-point bending test samples in Repetier-Host is shown below in Figure 30.

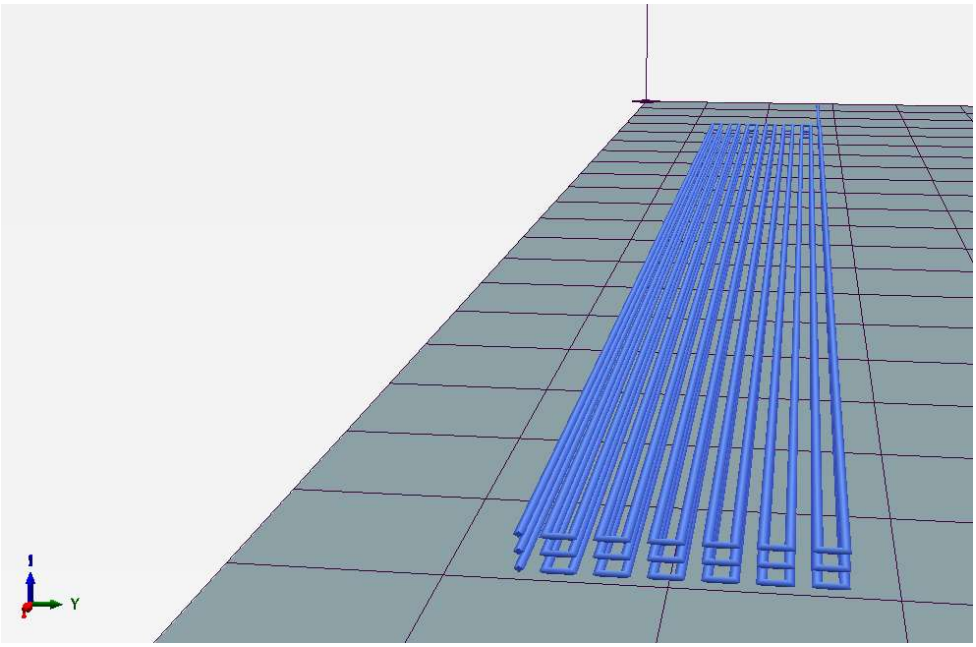

Figure 30: sliced 3k 3-point bending test model

One can note in Figure 30 above that the length of the 3k continuous carbon fiber reinforced 3-point bending test samples is greater than the other samples. This is due to the fact that the 3k fiber reinforced samples have a larger thickness; thus, in order to maintain the same span-to-depth ratio as the other samples, the length had to be increased.

The small 1-layer, 3-layer and 5-layer laminates had dimensions of 75 mm in length, 75 mm in width, and either 0.6, 1.8 or 3.6 mm in thickness, depending on how many layers were printed. These laminates were not fabricated to the specifications of any standard but were fabricated simply to establish consistency of layer height throughout the thickness of the prints. The samples only needed to be large enough so that any differences in thickness found near the

edges could be neglected, as thickness measurements would be taken towards the middle of the prints. The Solidworks 3D model for the 1-layer small laminate can be seen in Figure 31 below.

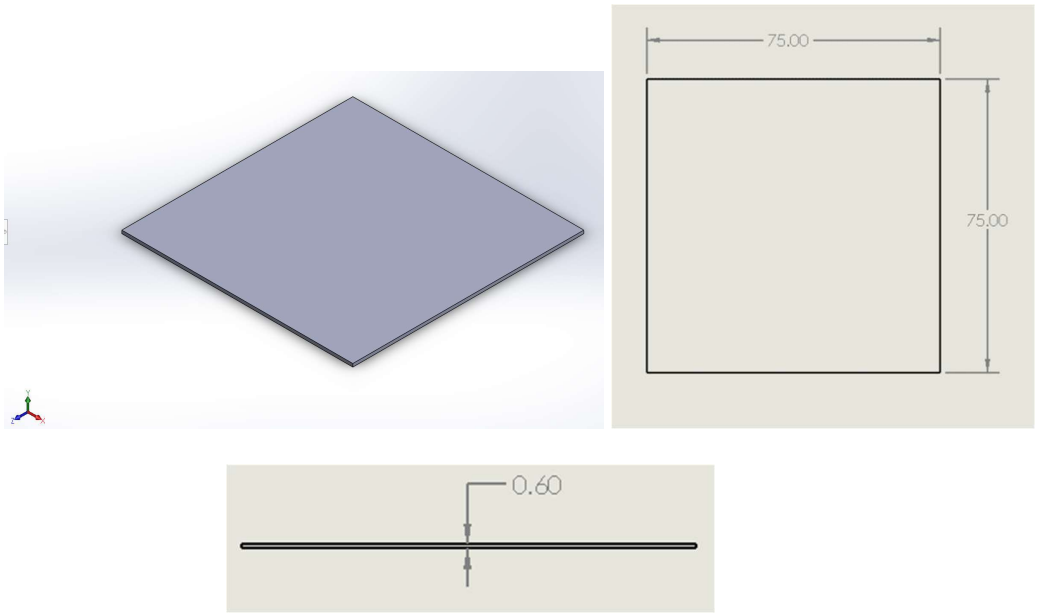

Figure 31: The 1-layer small laminate

These laminates were intended to be printed with both continuous 1k carbon fiber tow and pure PLA plastic, although this was not completed due to the campus shutdown after the coronavirus outbreak. The pure PLA laminates, however, were completed, and the sliced model of the pure PLA 1-layer laminate in Repetier-Host is shown below in Figure 32.

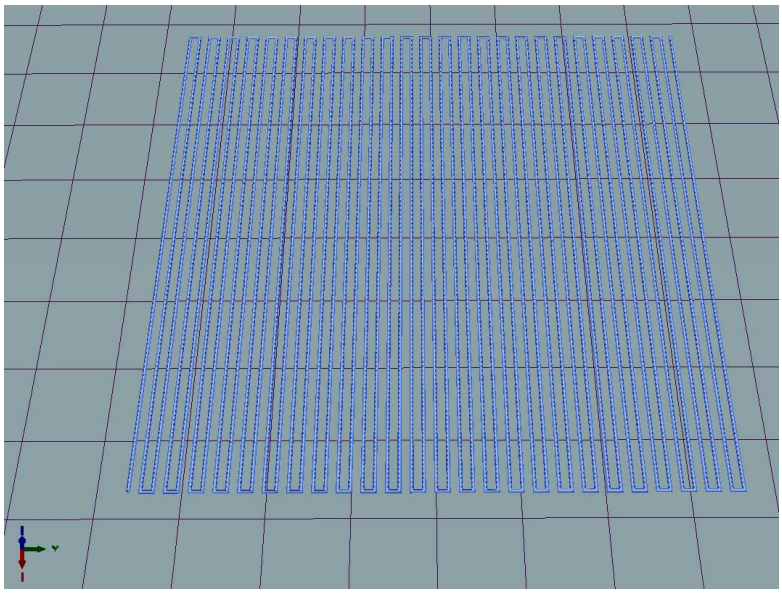

Figure 32: The sliced small 1-layer laminate model

The printing parameters of these small laminates are discussed in Section 4.2 below. Although the continuous 1k carbon fiber reinforced small laminates were not printed, a small 3-layer laminate using continuous 3k carbon fiber tow as reinforcement was successfully printed. This laminate used the same Solidworks 3D model shown in Figure 31 (with the thickness adjusted for that of a 3-layer laminate), although it was sliced differently than the pure PLA and 1k continuous carbon fiber reinforced laminates were. The slicing of the 3k continuous carbon fiber reinforced laminate differed from that of the pure PLA laminates in the same manner that the slicing of the 3k continuous carbon fiber reinforced 3-point bending test samples differed form that of the pure PLA and 1k continuous carbon fiber reinforced 3-point bending test samples, described above. The sliced 3k fiber small 3-layer laminate is shown below in Figure 33.

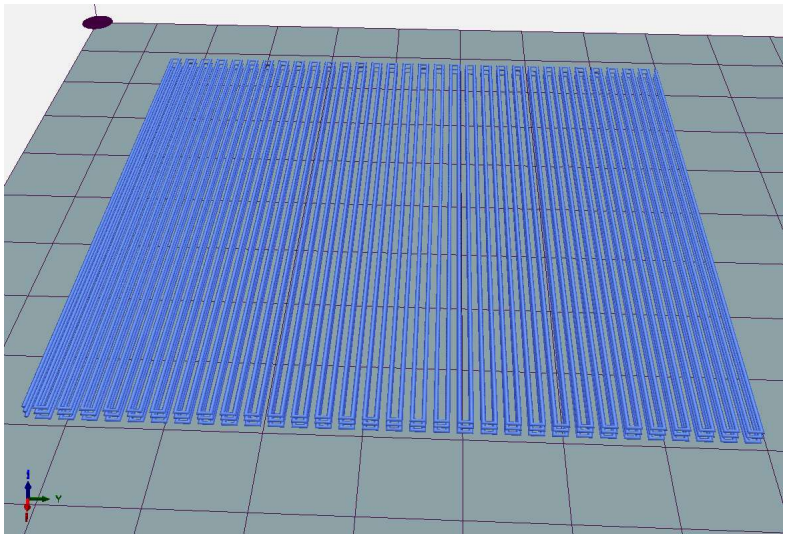

Figure 33: The sliced small 3-layer 3k fiber laminate model

After the small 1-, 3- and 5-layer laminates were printed, large 5-layer laminates were to be printed. Unfortunately, these large 5-layer laminates could not be fabricated because of the campus shutdown due to the coronavirus. Had they been fabricated, however, samples would have been cut from them and tested to determine the longitudinal and transverse modulus of the material. With this information, and verification of consistent layer height throughout the thickness of the print as provided by the smaller laminates, the modulus of a sample with any print orientation could be determined through laminate analysis.

Lastly, line samples were fabricated to provide characterization of the effect of layer thickness and nozzle temperature on the quality of print. The line samples were not fabricated to the specifications of any standard, but were simply single-line, one-layer thick prints fabricated to determine the effects of the two aforementioned print parameters. The Solidworks model for the line samples can be found in Figure 34 below.

Figure 34: The line samples model

The model shown in Figure 34 above was loaded into Repetier-Host and sliced. The sliced line sample model is shown in Figure 35 below.

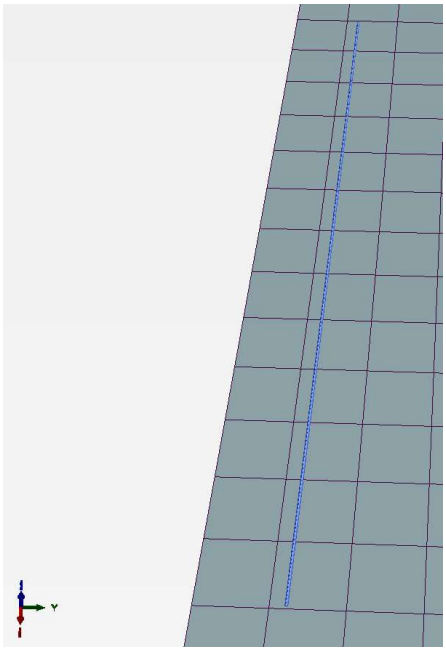

Figure 35: The sliced line sample model

The printing parameters for the line samples are discussed below in Section 4.2.

Section 4.2: Printing Parameters

There are numerous parameters that can be changed in the fused deposition modeling print process with the Creality CR-10 printer. Some of them are constant across all samples printed, and others change between different sample types. The parameters that are constant across all sample types are shown below in Table 2.

Table 2: Constant Print Parameters

Parameter	Value
Nozzle Diameter	1.5 mm
Extruder Temperature	230 degrees Celsius*
Bed Temperature	Room Temperature (Off)
Fan Speed	100%
Bed Adhesion Material	Elmer's Disappearing Purple Glue Stick

*Some line samples were not printed at 230 degrees Celsius for characterization purposes.

The nozzle diameter was the first parameter that had to be adjusted to ensure successful printing with the extrusion of continuous carbon fiber. A typical nozzle used in the fused deposition modeling of PLA plastic is 0.4 mm in diameter, but this is too small for simultaneously extruding PLA and carbon fiber. Work was published in 2017 in which 1k carbon fiber tow was printed along with ABS plastic through a single nozzle that was 0.8 mm in diameter [13]. In another work that was published in 2016, several thousand carbon fiber strands were taken from a 24k tow and simultaneously printed with PLA through a 1.4 mm-diameter nozzle [55]. A third work, published in 2017, prints 1k continuous carbon fiber tow and PLA through a single 2 mm-diameter nozzle [63]. These 3 works show the range of nozzle diameter found in the literature for the printing of continuous fiber and matrix through a single nozzle. This range is 0.8-2 millimeters. Thus, a 0.8

mm-diameter nozzle was first utilized, but this size did not allow for proper extrusion. A 1.0 mm-diameter nozzle was then utilized, but this size did not allow for proper extrusion either. A 2.0 mm-diameter nozzle was utilized, and this size allowed for proper extrusion but printed with very low print quality. Finally, a 1.5 mm-diameter nozzle was utilized, and this nozzle printed with good print quality while also allowing for proper extrusion. Thus, a 1.5 mm-diameter nozzle was implemented in this project.

The next parameter that must be adjusted to ensure successful printing is extruder temperature. Fused deposition modeling with PLA is typically performed with an extruder temperature of 200 degrees Celsius. With the addition of fiber, however, it is beneficial to increase the temperature of the extruder to decrease the viscosity of the PLA within the nozzle and consequently improve the impregnation of the fibers with PLA. It has been reported that the flexural strength and modulus are positively related to temperature up to 240 degrees Celsius in composites fabricated of PLA and 1k carbon fiber tow, with a recommended maximum temperature of 230 degrees Celsius [64]. Thus, an extruder temperature of 230 degrees Celsius was chosen for the printing of all samples in this project. One can note that several of the line samples were printed at temperatures that were not 230 degrees Celsius; this was done for characterization and these samples were not used to collect data. This is discussed later in this section.

Bed temperature is the next parameter that must be adjusted to ensure successful printing. Work has been reported in which several thousand strands of continuous carbon fiber were printed along with PLA on a bed that was heated to 80 degrees Celsius [55]. Thus, this was the first temperature attempted. In order to heat the bed to 80 degrees Celsius, the mosfet discussed in Chapter 2 above had to be employed. This bed temperature, however, did not work well, as the

first layer would warp off the bed. Much published literature on 3D printing with thermoplastic and continuous fiber does not use a heated bed, and therefore prints were attempted in this project without heating the bed. This helped adhesion immensely, and thus the bed was set at room temperature (or off) for the printing of all samples in this project.

Another parameter that must be adjusted to ensure successful printing is the bed adhesion material. This, along with bed temperature, is critical for proper adhesion of the print to the bed. The most common bed adhesion materials are painter's tape and glue stick, along with not using a bed adhesion material. A trial-and-error approach was employed to determine the best bed adhesion material to use in this project, and it was discovered that Elmer's Disappearing Purple glue stick works better than both painter's tape and no adhesion material. Thus, Elmer's Disappearing Purple glue stick was utilized as the bed adhesion material for all samples printed in this project.

Fan speed is yet another parameter that must be adjusted to ensure successful printing. The speed can be set anywhere from 0%-100% of the fans' full speed. It is important to note that this fan speed setting applies to both the nozzle cooling fan and the heat sink cooling fan. In the case of this project, there is no reason to not set the fan speed to 100%. A faster nozzle cooling fan speed means that extruded material solidifies quicker, and a faster heat sink cooling fan speed means that there is less of a chance for the PLA filament to melt above the heating block. The fan speed was therefore set at 100%, the fastest setting, for all prints fabricated in this project.

It is also important to note that there were no perimeters for any prints. A perimeter in 3D printing is the outer "shell" of a print, or the few rows of outer print that encompass the inner material on every layer. The samples printed in this project had no perimeters and were instead composed entirely of infill. The fill density was set to 99%, as the slicer settings do not allow for

100% fill density. 99% is therefore the closest fill density setting to completely solid. This fill density was used for every sample in this project. One can also note that the fill pattern for every print was “aligned rectilinear”. This is the pattern shown in Figure 29.

There were several printing parameters that were different depending on the sample type. These parameters are shown below in Table 3.

Table 3: Variable Print Parameters

Sample Type	**Layer Thickness (mm)**	**Extrusion Width (mm)**	**Hatch Spacing (mm)**	**Extrusion Multiplier**	**Nozzle Speed (mm/s)**
3-Point Bending Test (1k tow and pure PLA)	0.6	1.56427	1.45	0.875	1 (turns) or 2 (straightaways)
3-Point Bending Test (3k tow)	0.8	1.3	1.183	1.073	1
Small Laminate (Pure PLA)	0.6	1.56427	1.45	0.875	1

Small Laminate (3k tow)	0.8	1.3 mm	1.183	1.073	1
Large Laminate (Pure PLA)	0.6	1.56427	1.45	0.875	1
Line Samples	0.5, 0.6, 0.7, 0.8	N/A	N/A	1.75	1

The first parameter that is variable between sample types is layer height (or layer thickness). Literature has been published in which continuous fiber-reinforced thermoplastic composites were 3D printed with layer heights of 0.5 mm [13] and 1 mm [55]. One work investigated a range of layer heights from 0.3 mm to 0.8 mm and recommended a layer height of 0.4-0.6 mm, with maximum flexural strength occurring at 0.3 mm and decreasing with increasing layer height while fabrication efficiency increased with increasing layer height [64]. A trial-and-error approach was implemented in which line samples were printed with 1k fiber tow at layer heights of 0.5, 0.6, 0.7 and 0.8 mm to determine the optimal height. All of these layer heights were successful, but through printing multi-row, multi-layer samples, it was discovered that the fiber would consistently tear at layer heights below 0.6 mm. Thus, 0.6 mm was chosen as the layer height for all 1k fiber tow samples. The 3k fiber tow, being larger than the 1k tow, would tear at all layer heights below 0.8 mm. Thus, 0.8 mm was chosen as the layer height for all 3k tow samples.

Hatch spacing is another parameter that must be optimized for each sample type. Hatch spacing is the gap between rows of print. Through trial-and-error, it was initially found that 1.45 mm was the smallest the hatch spacing could be without the fiber tearing due to overlapping of rows. Thus, 1.45 mm was chosen as the value for hatch spacing for the 1k fiber-reinforced samples. The 3k fiber tow samples, however, had a larger layer height than the 1k samples while the same amount of material was extruded per unit length of print. This allowed for a smaller hatch spacing, and a value of 1.183 mm was chosen through trial-and-error.

Approximately 0.313 mm of PLA filament was extruded per 1 mm of print path for all samples except line samples. This value was chosen through trial-and-error. The extrusion width and extrusion multiplier parameters in Table 3 above both have direct influence over the amount of PLA filament extruded per mm of print. Thus, the values found in Table 3 above for these 2 parameters were found through trial-and-error to obtain the correct value of PLA filament extruded per mm. One can note that the line samples were printed with 0.68743 mm of PLA filament extruded per 1 mm of print path. This is the case because an optimal value had not yet been established for PLA filament extrusion. This value, however, was not relevant to the printing of the line samples, as they were only printed to investigate the effect of layer height and extrusion temperature.

Nozzle speed was the last print parameter that was variable between sample types. The nozzle speed was kept at 1 mm/s for all laminates printed and for the 3k tow 3-point bending samples. This was due to the fact that this is the only speed at which 3k fiber was successfully printed and that it is better to print at a safer speed for larger laminates. For the pure PLA and 1k fiber 3-point bending test samples, however, a speed of 2 mm/s was used for the straightaways whereas a speed of 1 mm/s was used for the turns.

Section 4.3: 3-Point Bending Test Samples

5 pure PLA 3-point bending samples and 5 1k carbon fiber reinforced PLA 3-point bending samples were tested. An image of each of these types of samples can be found in Figure 36 below.

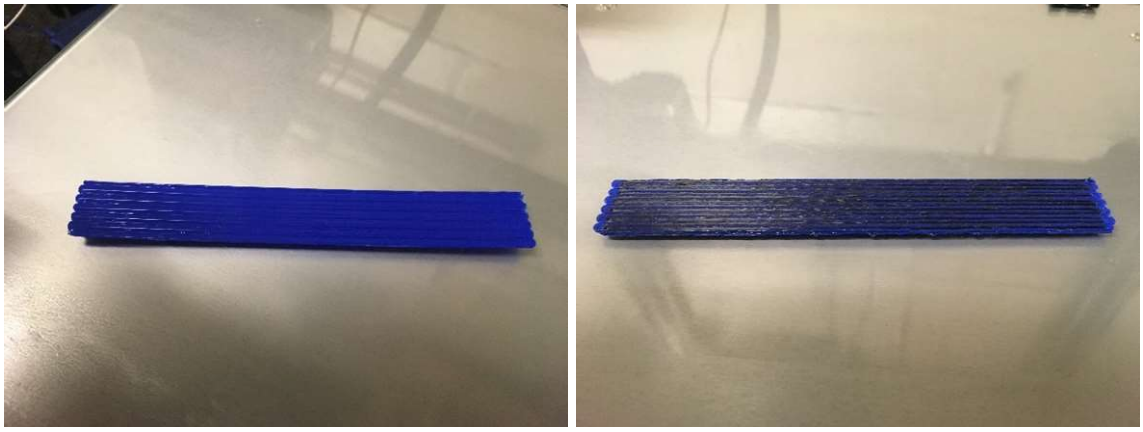

Figure 36: Pure PLA and 1k fiber samples

The samples took roughly 45 minutes to print and were all 3 layers in height. The most critical step in the process of printing these samples is the first layer. If bed adhesion is poor, the first layer will warp off the print bed and obstruct the printing of subsequent layers while altering the dimensions of the sample. Through utilization of Elmer's Disappearing Purple glue stick and through not heating the bed, however, proper bed adhesion was achieved. At the beginning of the print, the single line of print (as shown in Figure 27) had to be manually clamped onto the bed for a few seconds to establish bed adhesion and fiber tension. After a few seconds, however, the sample could be let go, and the tension provided by the already-solidified print would be enough to continuously pull the fiber through the nozzle.

Multiple 3k fiber tow-reinforced 3-point bending test samples were fabricated, although not enough were fabricated to be tested due to campus closure. The printing process for these samples was the same as the printing process for the 1k fiber samples except for how the printing speed was 1 mm/s for the entire print and thus the sample took over an hour to fabricate. The 3k

fiber tow-reinforced samples were 3 layers in height as well. An image of a 3k fiber tow-reinforced sample can be seen below in Figure 37.

Figure 37: A 3k fiber sample

Section 4.4: Laminates

A full set of laminates was not printed due to the campus closure because of the coronavirus. Small pure PLA and 3k fiber tow-reinforced laminates, however, along with large pure PLA laminates, were fabricated. The small laminates were fabricated with the purpose of taking thickness measurements at several different locations to verify consistent layer height across all layers. The thickness measurements were not taken due to campus closure, but 1-layer and 3-layer pure PLA and 3k fiber-reinforced laminates were successfully fabricated. These laminates had dimensions of 75 mm in length and 75 mm in width. The layer height was 0.8 mm. A 3-layer pure PLA and 3-layer 3k fiber-reinforced PLA small laminate can be seen in Figure 38 below.

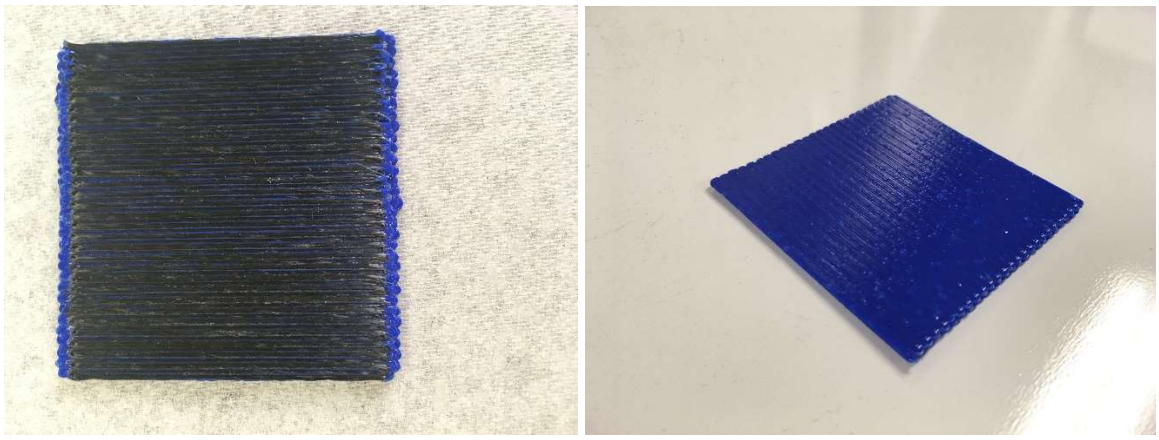

Figure 38: Small 3-layer laminates

Large pure PLA laminates were also fabricated with the purpose of having 3-point bending test samples cut from them once layer height consistency was established throughout the thickness of the smaller laminates. From the cut samples, values for longitudinal and transverse modulus of the material could be calculated and used to predict theoretical modulus values of samples with any fiber/PLA orientation. Large laminates were not printed with any form of reinforcement and samples were not cut from the large pure-PLA sample, however, because of the campus closure.

Section 4.5: Line Samples

Early on in this project, line samples were fabricated to provide characterization of the effect of layer height and nozzle temperature on impregnation of the fibers in 1k tow with PLA. This is not the first time this type of characterization has been performed. Work was published in 2018 in which line samples were printed of PLA, ABS (acrylonitrile butadiene styrene), PET (polyethylene terephthalate) and PP (polypropylene) to determine the effects of print speed and temperature on print quality [65]. The PLA line samples were fabricated at every combination of temperatures from 160-200 degrees Celsius in increments of 10 degrees and speeds from 5-50 mm/s in increments of 5 mm/s [65]. A similar approach was taken in this project to determine the

optimal temperature and layer height at which to print. The different combinations of parameters are shown below in Table 4.

Table 4: Line Sample Parameters

Sample Number	Thickness (mm)	Nozzle Temperature (degrees Celsius)
1	0.5	200
2	0.6	200
3	0.7	200
4	0.8	200
5	0.5	215
6	0.6	215
7	0.7	215
8	0.8	215
9	0.5	230
10	0.6	230
11	0.7	230
12	0.8	230

One can note that all of the line samples were printed with a speed of 1 mm/s and were printed using the 1k carbon fiber tow. Once the samples were printed, they were pulled apart in a tensile testing machine to show the level of fiber pullout in each sample. Less fiber pullout means better impregnation of the fibers, whereas more fiber pullout means worse impregnation of the fibers. The results of this fiber pullout testing are shown below in Figure 39.

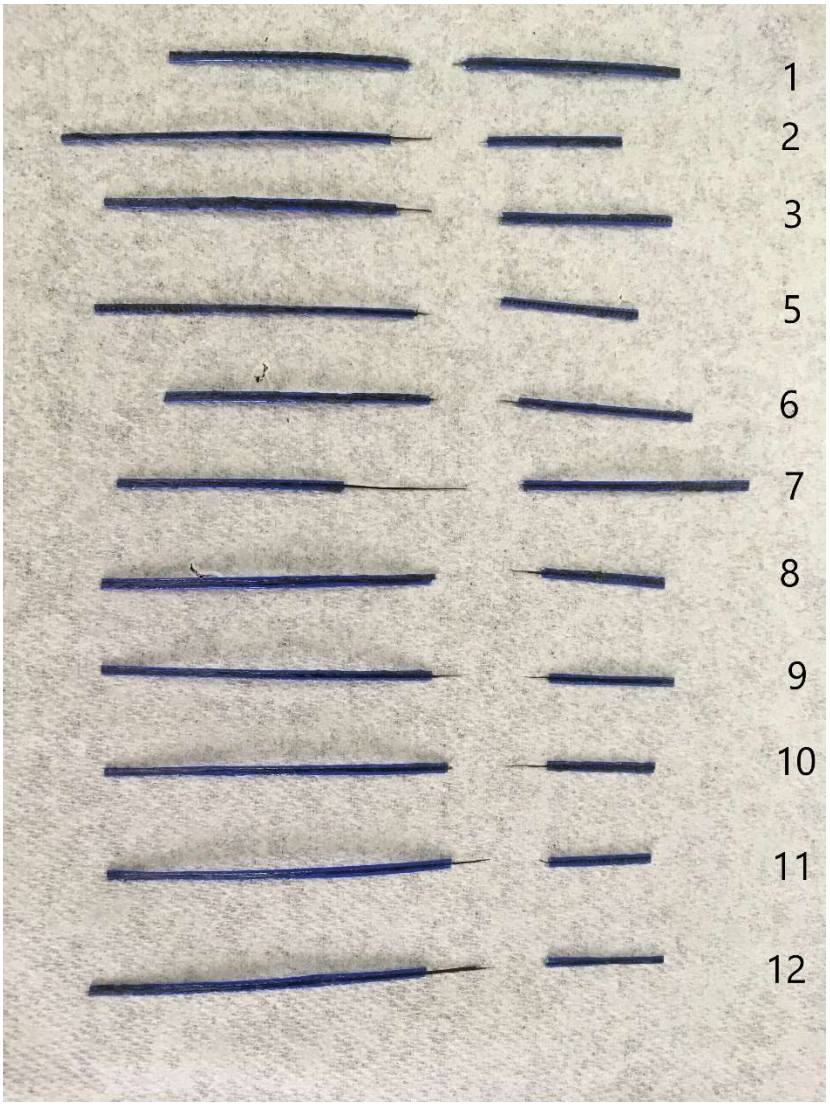

Figure 39: Fiber pullout testing results

As one can observe in Figure 39 above, there are no results for Sample 4. This is because the sample was lost and there was not enough time to print and test another one before the campus closure. Nevertheless, one can observe that the least amount of carbon fiber pullout occurs in the line samples with the smallest layer height, or the samples with a layer height of 0.5 mm. There is no recognizable trend in the amount of fiber pullout as temperature changes. Thus, one can conclude from this characterization that it is optimal to print with the smallest layer height that

does not result in tearing the fiber. That value is 0.6 mm for 1k fiber-reinforced PLA and 0.8 mm for 3k fiber-reinforced PLA.

Section 4.6: Measurement and Geometry Shape Validation

The 3-point bending test samples that were tested in this project were fabricated according to ASTM standard D790. As previously discussed, this standard recommends that high strength reinforced composites have a span-to-depth ratio of 32:1 or 40:1 along with a rectangular cross-section. Table 5 below shows the theoretical dimensions of the samples as set in Solidworks.

Table 5: 3-Point Bending Test Samples Theoretical Dimensions

	Length (mm)	**Width (mm)**	**Height (mm)**
Pure PLA	124.0	16.0	1.8
1k Fiber-Reinforced	124.0	16.0	1.8

The actual dimensions of the samples were measured with a dial caliper. Each dimension was measured at 3 different locations on the sample. The locations of each measurement are shown in Figure 40 below.

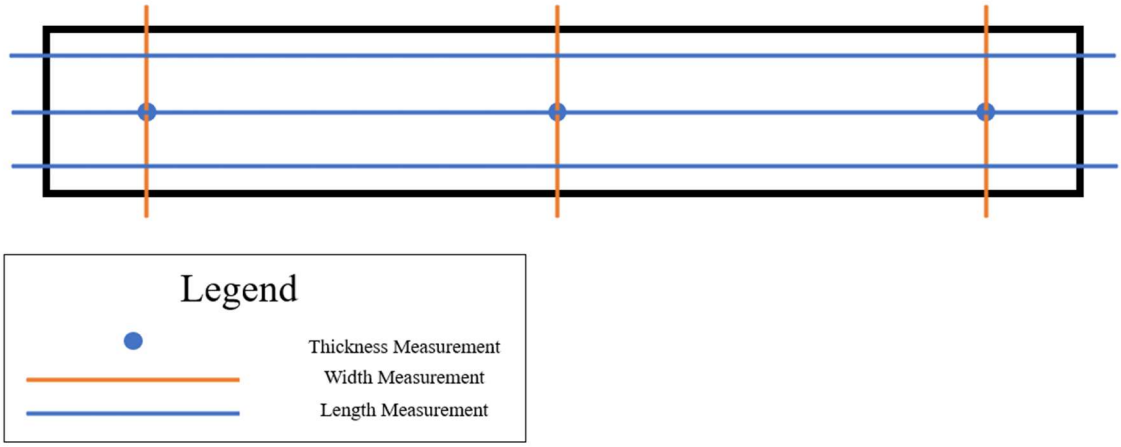

Figure 40: Location of measurements

Measurements for length, width and thickness were taken for all 5 pure PLA and all 5 1k carbon fiber tow-reinforced PLA samples fabricated. The average values for these measurements for each sample type are shown below in Table 6.

Table 6: 3-Point Bending Test Samples Measured Dimensions

	Length (mm)	**Width (mm)**	**Height (mm)**
Pure PLA	124.0	17.8	2.0
1k Fiber-Reinforced	123.9	18.2	2.1

One can observe that for the pure PLA samples, the measured length is equal to the theoretical length, the measured width is larger than the theoretical width, and the measured thickness is larger than the theoretical thickness. This increase in width is likely due to the molten PLA spreading outward before solidification, whereas the increase in thickness could be due to small ridges that formed between rows of print. One can observe that for the 1k carbon fiber tow-reinforced samples, the measured length is slightly less than the theoretical length, the measured

width is larger than the theoretical width, and the measured thickness is larger than the theoretical thickness. The difference in measured length and theoretical length is not considered to be significant. The increase in measured width from theoretical width is likely due to much spreading of PLA upon extrusion, particularly because of the carbon fiber being fed through the nozzle along with the PLA. The increase in height is likely caused by the same reason; the carbon fiber being fed through the nozzle along with the PLA probably forced some material to the sides upon extrusion, and this material likely solidified above the nozzle height. There were small ridges present between rows, just as there were in the pure PLA samples. These ridges were probably caused by the excess material being pushed to the side upon extrusion and likely accounted for some of the additional height.

Chapter 5: Mechanical Testing of 3D Printed Samples

Section 5.1: Density Measurements

The first of the mechanical testing that was performed on the printed 3-point bending samples was the 3-point bending tests, which are detailed below in Section 5.3. After the 3-point bending tests were performed, however, density measurements were taken. These measurements were taken via a density cup and a gas pycnometer.

The density cup method is based on Archimedes Principle and can be used to determine the density of a known mass. The first step is to take the mass of the density cup alone and record the value. The lid of the cup is then removed, and the cup is filled with water before the lid is placed back on the cup. Excess water will exit the cup through the hole in the lid, and this water is absorbed with a paper towel. The density cup filled with water is then massed again. The next step in this process is to take the mass of the sample. In the case of this project, a section was cut from each of three pure PLA 3-point bending test samples and three 1k carbon fiber-reinforced 3-point bending test samples. The cut section was massed, and the mass value was recorded for each sample before the cut section of each sample was placed in the density cup. Again, excess water exited the density cup through the hole in the lid when the lid was placed back on the cup, and this excess water was absorbed with a paper towel. The density cup was then massed again with the sample and water inside. One must then use the following equations to calculate the volume and density of the sample. First, one must use the equation below to determine the volume of the water.

$$m_{dcw} = \rho_w v_w + m_{dc}$$

In the equation above, m_{dcw} is the mass of the density cup with the water in it, ρ_w is the density of the water, v_w is the volume of the water and m_{dc} is the mass of the density cup alone.

All these values are known except for the volume of the water, and thus it is simple to obtain this value from the above equation. The next step is to determine the volume of the sample, which can be done using the equation below.

$$m_{dcw+s} = \rho_w(v_w - v_s) + m_s + m_{dc}$$

In the equation above, m_{dcw+s} is the mass of the density cup with the water and sample inside, v_s is the volume of the sample and m_s is the mass of the sample. All these values are known expect for the volume of the sample, and thus it is easy to calculate this value using the above equation. The last step is determining the density of the sample. This is done using the equation below.

$$m_s = v_s\rho_s$$

In the above equation, ρ_s is the density of the sample. The mass and volume of the sample are known by this point, and the density can, therefore, be easily calculated. This process was carried out to calculate the density of both pure PLA and 1k carbon fiber-reinforced PLA samples 3-point bending test samples.

The second method used in this project to determine the density of the samples is the gas pycnometer method. A gas pycnometer functions by determining the pressure change in a chamber due to the displacement of gas by a solid object. This is accomplished by first expanding a quantity of gas at a known pressure into the chamber that is initially empty. Measuring the pressure of the gas in the chamber at this point establishes a baseline. A sample is then placed into the chamber before the chamber is sealed back off. The same quantity of gas is expanded into the chamber again at the same pressure as the first time, and the pressure is measured again. The difference in the two pressure measurements along with the known volume of the empty chamber enables the

volume of the sample to be determined via the ideal gas law. The gas pycnometer is generally a more accurate method of measuring density than the density cup is, although one must note that the effectiveness of the gas pycnometer relies greatly on the cleanliness of the sample and the purity of the gas pumped into the chamber. The gas pycnometer was utilized to determine the density of both pure PLA 3-point bending test samples and 1k carbon fiber-reinforced 3-point bending test samples.

The densities of the samples as determined by both methods detailed above are shown below in Table 7.

Table 7: Density Measurements

Sample Name	**Density Cup Method Density (g/cm^3)**	**Gas Pycnometer Method Density (g/cm^3)**
Pure PLA Sample 3	1.177	1.292
Pure PLA Sample 4	1.203	1.280
Pure PLA Sample 5	1.157	1.306
1k Fiber-Reinforced Sample 3	1.017	1.228
1k Fiber-Reinforced Sample 4	1.069	1.223
1k Fiber-Reinforced Sample 5	1.188	1.224

As one can observe in Table 7 above, the density of the pure PLA samples is measured via density cup to be between 1.15 and 1.21 g/cm^3 and measured via gas pycnometer to be between

1.28 and 1.31 g/cm^3. The density of the 1k carbon fiber-reinforced samples is measured via density cup to be between 1.02 and 1.19 g/cm^3 and measured via gas pycnometer to be between 1.22 g/cm^3 and 1.23 g/cm^3. For both sample types, the gas pycnometer measured higher density values than the density cup. The gas pycnometer is regarded as the more accurate method, and the ranges of values measured by the gas pycnometer are therefore considered to be the more accurate density values. In both measurement methods, however, the pure PLA samples have higher density. One can note that the density cup measurement for 1k fiber-reinforced sample 5 is considered as an outlier. Another measurement was going to be taken, but campus closed due to the coronavirus before the procedure could be undertaken. Nevertheless, the pure PLA samples have higher density than the fiber-reinforced samples. This is surprising, as PLA has a density of 1.24 g/cm^3 [66] whereas carbon fiber has a density of 1.75-2.00 g/cm^3 [67]. With carbon fiber having a higher density, one would expect the fiber-reinforced samples to have a higher density than the pure PLA samples. A possible explanation for why the fiber-reinforced samples have lower density could be increased porosity when compared to the pure PLA samples.

Section 5.2: Resin Burn Off Test and Fiber Volume Fraction Measurements

An important characteristic that is considered in fiber-reinforced composites is fiber volume fraction. Fiber volume fraction is the fraction of the total volume of a composite that consists of the fiber reinforcement. The higher the fiber volume fraction, the better the material properties of the composite. The highest realistic fiber volume fraction is around 70% [68]. The highest theoretical fiber volume fraction is around 90%, but this is not realistically achievable due to manufacturing limitations. One would not want to have too high of a fiber volume fraction anyways, however, as too high of a fiber volume fraction can actually decrease the strength of a composite due to the matrix not having enough space to completely surround and impregnate the

fibers [69]. Adding too little fiber reinforcement can decrease the strength of a composite as well, and thus there is a balance that one must account for with an optimal fiber volume fraction.

To determine the fiber volume fraction of the 1k fiber-reinforced 3-point bending test samples printed in this project, the resin burn-off method was employed. In this method, one first takes the mass of neat fiber (with PLA/chloroform coating and manufacturer sizing applied) and the mass of a fiber-reinforced sample. One then places both in a furnace and leaves them there for 5 hours at 450 degrees Celsius. An image of both neat fiber and a fiber-reinforced sample in the furnace is shown in Figure 41 below, with the neat fiber shown within the red box whereas the fiber-reinforced sample is shown within the blue box.

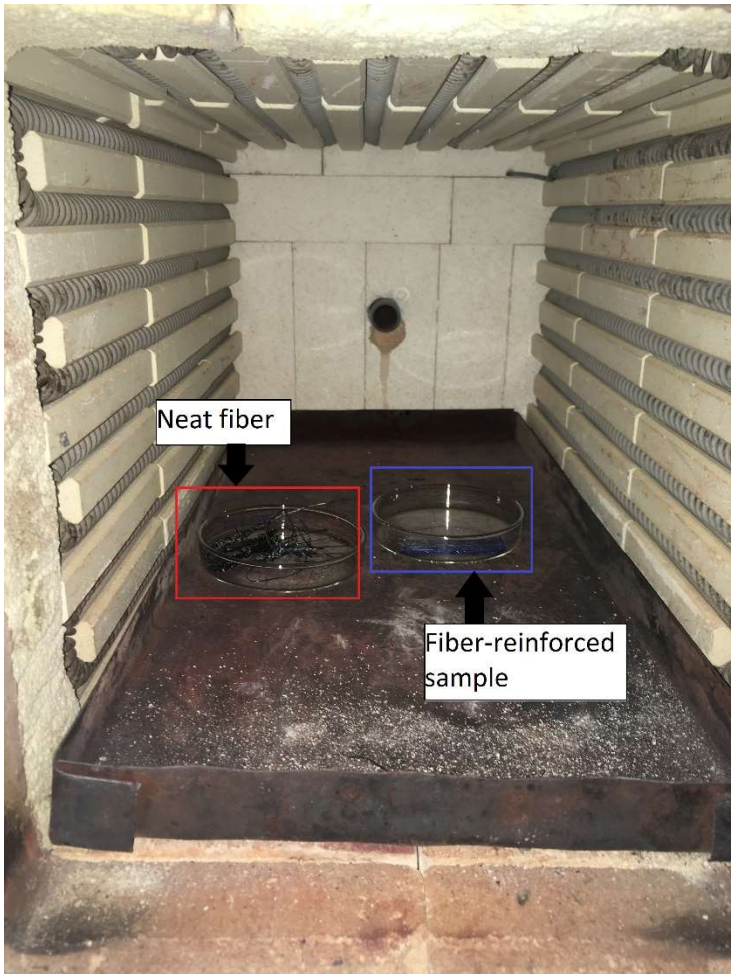

Figure 41: Neat fiber and a sample in the furnace

After removal from the furnace, the PLA/chloroform coating and the manufacturer sizing have been burned off from the neat fiber whereas the PLA matrix has been burned off from the fiber-reinforced composite. The remaining fiber is then massed for both cases, and the fiber volume fraction calculations can subsequently be made.

One must first determine the mass fraction of the manufacturer sizing and PLA/chloroform coating in the coated neat fiber. This starts with the equation

$$\Delta m_f = m_{fi} m_{ff}$$

where Δm_f is the difference in mass of the fiber from pre-burn-off to post-burn-off, m_{fi} is the initial mass of the fiber pre-burn-off, and m_{ff} is the final mass of the fiber post-burn-off. One can then determine the mass fraction of the PLA/chloroform coating and manufacturer sizing by using the equation

$$f_s = \frac{\Delta m_f}{m_{fi}}$$

where f_s is the mass fraction of the PLA/chloroform coating and manufacturer sizing.

One may use this information to help interpret the data from the burn-off test of the fiber-reinforced composite sample. In the burn-off test of the fiber-reinforced composite sample, one starts with the equation

$$m_c = m_f \left(1 + \left[\frac{1}{1 - f_s}\right] f_s\right) + m_r$$

where m_c is the original mass of the composite sample, m_f is the mass of the fiber after burn-off test of the composite sample, and m_r is the mass of the resin from the original composite sample. m_c, m_f, and f_s are all known quantities, and thus this equation can be used to solve for m_r. One can then determine the total volume of resin in the composite by using the equation

$$V_r = \frac{m_r}{\rho_r}$$

where V_r is the volume of the resin from the original composite sample and ρ_r is the density of the resin. The volume of the entire composite can be calculated in the same manner using the equation

$$V_c = \frac{m_c}{\rho_c}$$

where V_c is the volume of the original composite sample and ρ_c is the density of the original composite sample. One can note that the density value for the sample is obtained through the density measurements described in Section 5.1 above. One can then use the equation

$$V_c = V_f + V_r$$

where V_f is the volume of the fiber and its PLA/chloroform coating and manufacturer sizing. One may then divide the above equation by V_c to obtain

$$1 = v_f + v_r$$

where v_f is the volume fraction of the fiber (including PLA/chloroform coating and manufacturer sizing) and v_r is the volume fraction of the resin. The volume fraction of the resin is already known, as V_c and V_r have already been calculated. Thus, the volume fraction of the coated fiber can be calculated. The value obtained for the volume fraction of the coated fiber for one of the 1k fiber-reinforced 3-point bending test samples was 0.1186, or 11.86%. To determine the volume fraction of the pure fiber without the PLA/chloroform coating or manufacturer sizing, one must simply multiply this fraction by f_s. In doing so, the volume fraction of the pure fiber was calculated to be 0.0990, or 9.90%. One must note that these volume fraction values do not account for voids. Both of these values are low, and thus increasing the fiber volume fraction is included in the future work of this project, discussed in Chapter 6 below.

Section 5.3: 3-Point Bending Testing of 3D Printed Samples

There were 5 pure PLA samples and 5 1k carbon fiber tow-reinforced samples printed for utilization in the 3-point bending test for this project. The samples, after being measured, were loaded into an Instron 3345 single-column mechanical testing machine. An image of a 3-point bending test sample loaded into the machine is shown below in Figure 42.

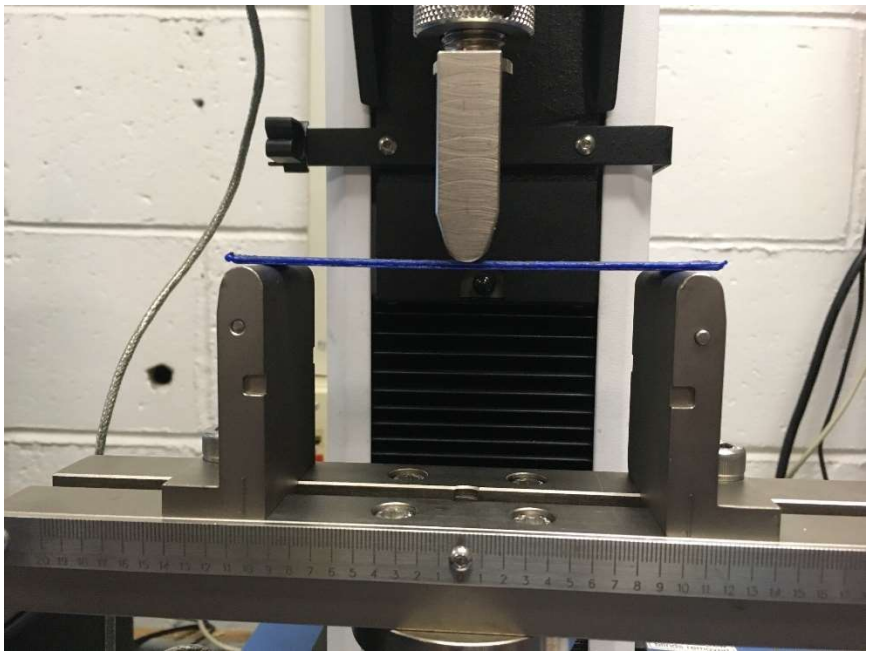

Figure 42: A sample loaded into the 3-point bending test apparatus

A desktop computer was connected to the machine and Instron software was used to conduct the testing. Testing was conducted in accordance with ASTM standard D790. The support span was roughly 103 mm for all samples, and the crosshead speed, which was calculated for each sample based on the support span, depth of the sample and strain rate of the outer fiber in the sample, was equal to between 8.5 and 9 mm/min for each sample. It is important to note that ASTM standard D790 distinguishes between 3 different possible stress-strain curves for samples. An image of this discernment is shown below in Figure 43.

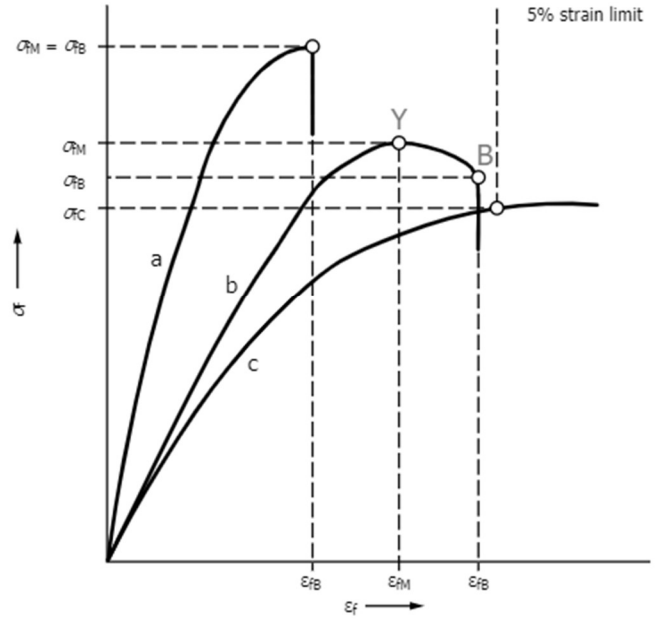

Figure 43: Typical curves of flexural stress vs. flexural strain [70]

Curve "a" in Figure 43 above represents a specimen that breaks before yielding. Curve "b" represents a specimen that yields and then breaks before the 5% strain limit. Curve "c" represents a specimen that neither yields nor breaks before the 5% strain limit. In the case of the 1k fiber tow-reinforced composite samples, every sample yielded but did not break before the 5% strain limit. Thus, they were treated as samples of the same type as curve "b" in Figure 43. ASTM Standard D790 states that for samples that do not break at strains of up to 5% but give a yield point, the flexural strength may be calculated by letting the loading equal that of the yield point [70]. Thus, the maximum stress sustained by each sample at strains up to the 5% limit was taken as the fracture stress. ASTM Standard D790 also stipulates that if the span-to-depth ratio of a simple supported beam during 3-point bending testing is greater than 16 to 1, such that beam deflections are greater than 10% of the support span, significant end forces can develop at the top of the supports that affect the moment in the beam [70]. Influence of these end forces is addressed with an approximate correction factor that allows for reasonable approximation of the stress in such beams [70]. The

typical equation for calculating stress resulting from 3-point bending testing as stated by ASTM Standard D790, without the aforementioned correction factor, is

$$\sigma_f = 3PL/2bd^2$$

where σ_f is the stress in the outer fibers at the midpoint (in MPa), P is the load at a given point on the load-deflection curve (in N), L is the support span (in mm), b is the width of the beam (in mm) and d is the depth (or thickness) of the beam (in mm) [70]. The modified equation including the correction factor as stated by ASTM Standard D790 is

$$\sigma_f = (3PL/2bd^2)[1 + 6(D/L)^2 - 4(d/L)(D/L)]$$

where D is the deflection of the centerline of the specimen at the middle of the support span (in mm) [70]. This equation that includes the correction factor was utilized in the calculation of stress for all fiber-reinforced PLA 3-point bending test samples that were tested in this project. An image of the stress-strain plot for the 5 fiber-reinforced samples is shown below in Figure 44.

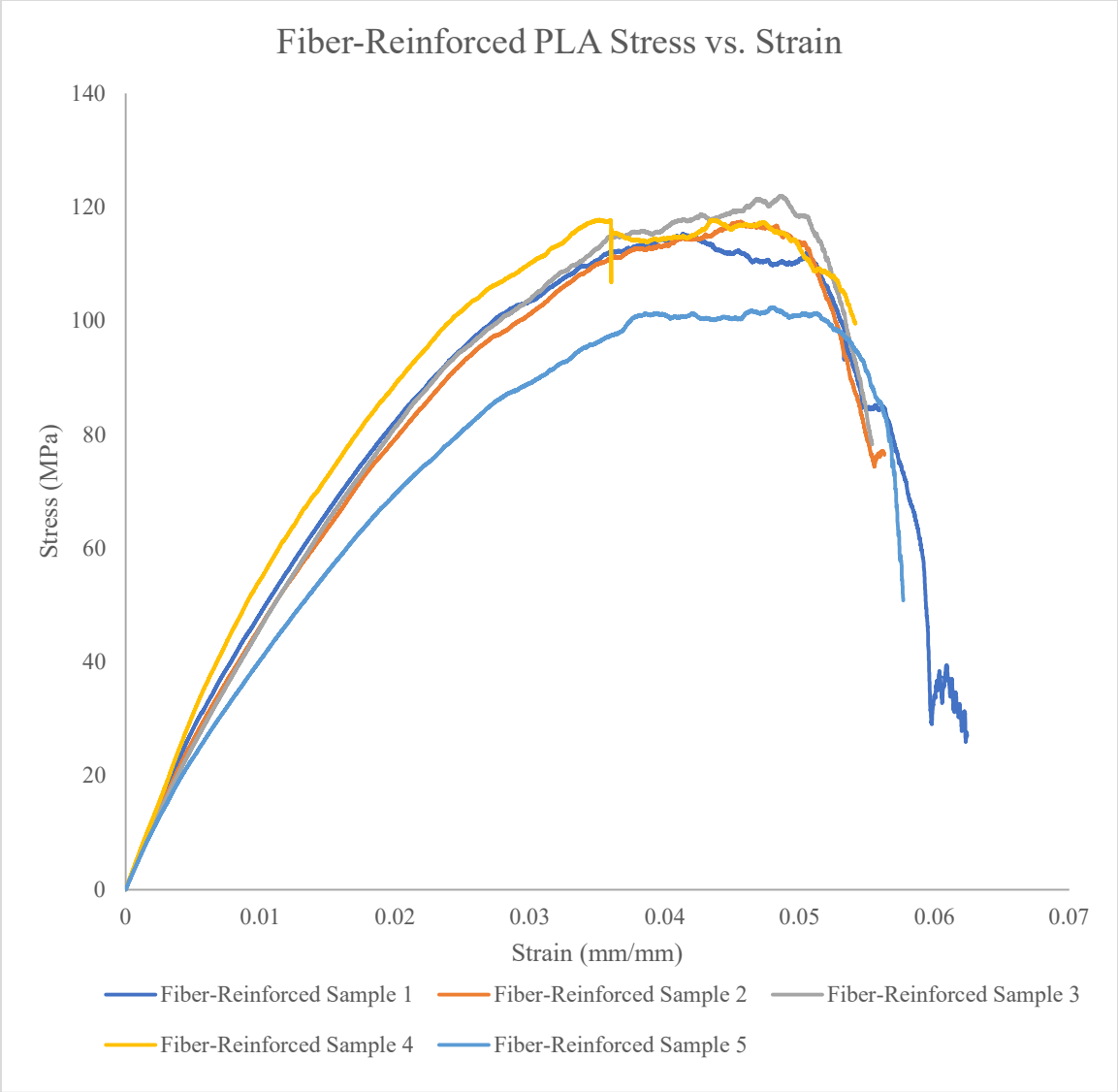

Figure 44: The stress vs. strain plot for the reinforced samples

As one can observe in Figure 44 above, the stress-strain curves exhibit good overall consistency across all 5 samples, indicating good repeatability for this experiment. One can also observe that no sample had a clean break. The samples instead underwent a gradual yielding process that began before the 5% strain limit for each sample. This yielding can be seen in Figure 45 below.

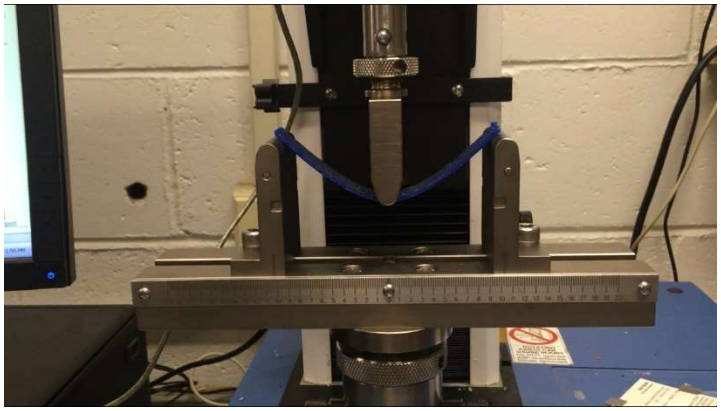

Figure 45: Yielding of reinforced sample

The picture shown in Figure 45 above was taken towards the end of a 3-point bending test when the sample was approaching the 5% strain limit. One can observe that the sample is simply too flexible to encounter a clean fracture. Nevertheless, the maximum stress sustained up to the 5% strain limit and the elastic modulus calculated for each sample are shown below in Table 8.

Table 8: Fracture stress and elastic modulus of reinforced samples

Sample Name	**Fracture Stress (MPa)**	**Elastic Modulus (GPa)**
1k Fiber-Reinforced Sample 1	115.310	5.902
1k Fiber-Reinforced Sample 2	117.464	5.727
1k Fiber-Reinforced Sample 3	122.019	5.934
1k Fiber-Reinforced Sample 4	117.828	6.391
1k Fiber-Reinforced Sample 5	102.413	5.401

The elastic modulus values shown above were taken at 0.1% strain. This was to ensure that the slope of the stress vs. strain curve was constant for these calculations.

The pure PLA samples, like the 1k fiber tow-reinforced samples, all yielded before the 5% strain limit without breaking before the limit. The maximum stress sustained by each sample up to the 5% strain limit was therefore taken to be the fracture stress again, with the stresses again calculated utilizing the equation with the correction factor shown above. The stress vs. strain plot for the 5 pure PLA samples tested is shown below in Figure 46.

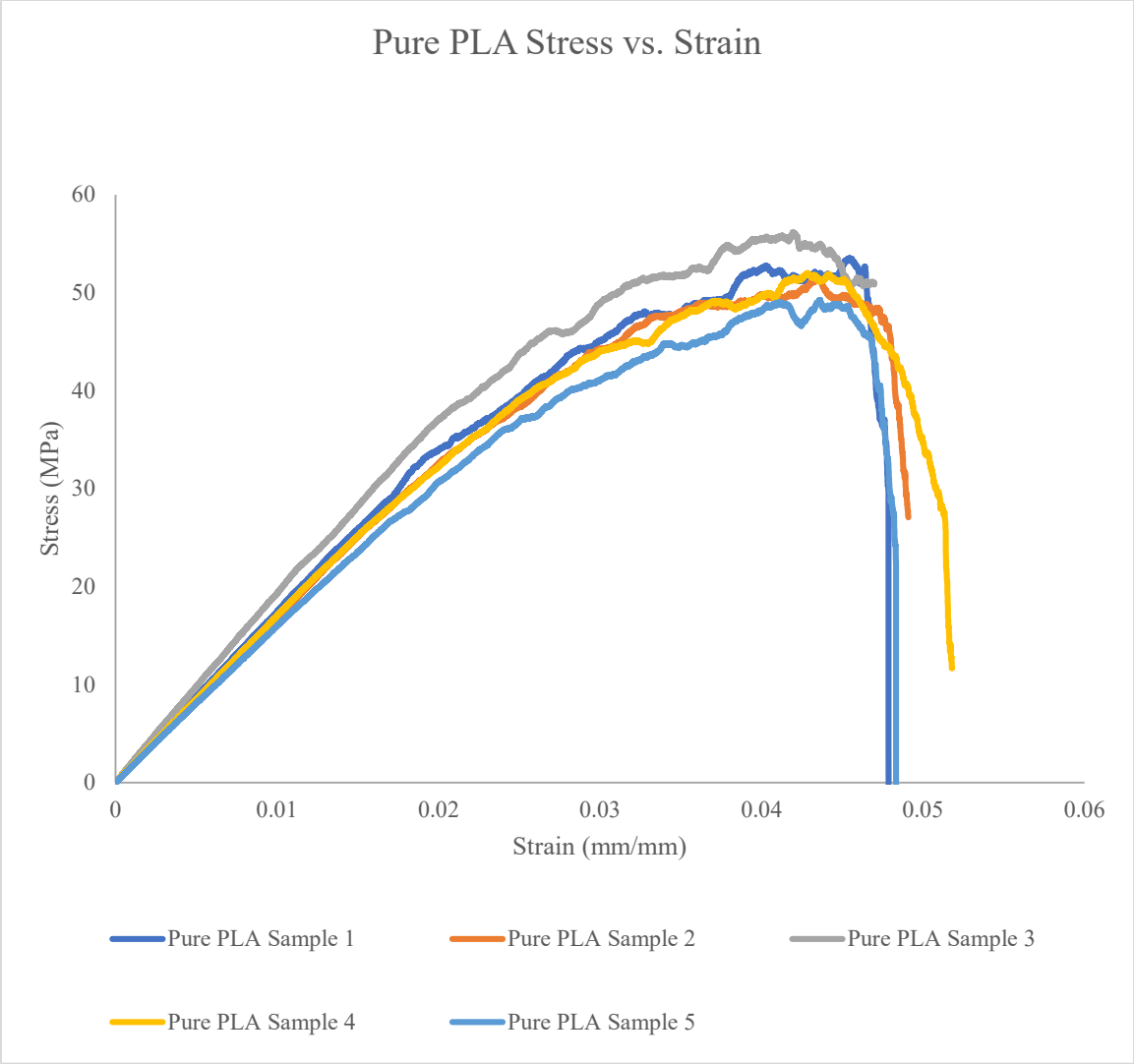

Figure 46: The stress vs. strain plot for the pure PLA samples

In Figure 46 above, one can observe good consistency in the stress-strain curves across all 5 pure PLA samples, again indicating good repeatability for this experiment. Some of the samples shown in Figure 46 appear to exhibit a clean break. This is not the case, as these samples actually slipped entirely off of the mounts during testing due to their flexibility. An image of one of these samples towards the end of the test is shown below in Figure 47.

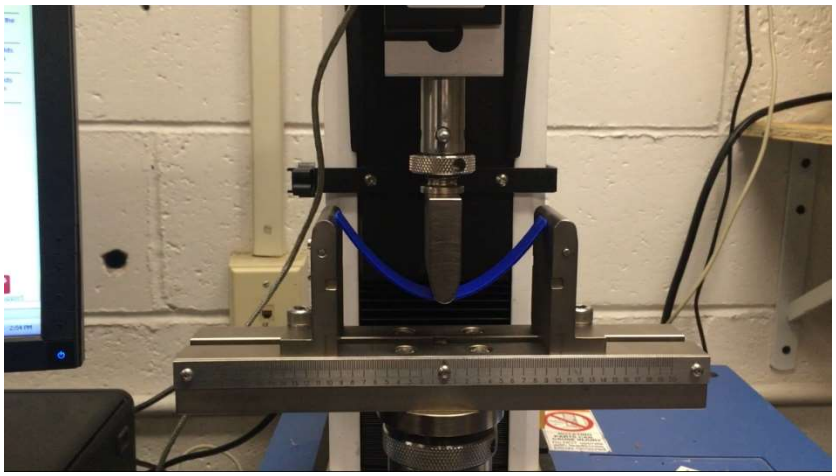

Figure 47: A pure PLA sample slipping off of the mounts

Shortly after the picture in Figure 47 was taken, the sample slipped entirely off of the mounts and the load consequently went to 0. The maximum stress sustained up to the 5% strain limit and the elastic modulus calculated for each sample are shown below in Table 9.

Table 9: Fracture stress and elastic modulus of pure PLA samples

Sample Name	Fracture Stress (MPa)	Elastic Modulus (GPa)
Pure PLA Sample 1	53.519	1.752
Pure PLA Sample 2	51.537	1.752
Pure PLA Sample 3	56.169	2.057
Pure PLA Sample 4	51.993	1.732
Pure PLA Sample 5	49.269	1.681

The elastic modulus values shown in Table 9 above were taken at 0.1% strain for the same reason that the elastic modulus values for the fiber-reinforced samples were.

The average fracture stress for the 5 fiber-reinforced samples was 115.007 MPa, whereas the average fracture stress for the 5 pure PLA samples was 52.497 MPa. This means that the

average fracture stress for the fiber-reinforced samples was about 219% of the average fracture stress of the pure PLA samples. This is a sizeable jump, yet this data is difficult to compare to other data because the 1k carbon fiber tow was purchased from eBay and thus the material properties of the 1k carbon fiber tow are unknown. Samples were to be printed and tested with 3k fiber of which the material properties were known, but this process was not started due to the campus closure. The average elastic modulus value of the fiber-reinforced samples was 5.871 GPa, whereas the average elastic modulus value of the pure PLA samples was 1.795 GPa. This is a sizeable jump, yet these values cannot be easily compared to other data for the same reason that the fracture stress data cannot be easily compared to other data. Nevertheless, the increase in sustained fracture stress values and elastic modulus values observed in the fiber-reinforced composite samples from the pure PLA samples is promising.

Chapter 6: Conclusions and Future Work

In this project, continuous carbon fiber-reinforced PLA composite samples were 3D printed and tested to study their mechanical properties. A commercially bought Creality CR-10 3D printer was modified to enable the feeding of continuous carbon fiber tow directly into the hot end of the printer, prior to melting of the PLA plastic. To prevent fraying of the fiber within the nozzle and easy breaking, the fiber was coated with a mixture of scrap PLA and chloroform in a novel process. Parameters such as print speed, layer height, hatch spacing, extrusion temperature, bed temperature, extrusion multiplier and bed adhesion material were all optimized through experimentation to produce the highest-quality samples. Single-line samples were printed at various temperatures and thicknesses to characterize the effects of these parameters, and it was concluded that a lower layer height is better for impregnation of the carbon fiber by the PLA matrix. 3-point bending test samples were printed of 1k carbon fiber tow-reinforced PLA plastic and pure PLA plastic. Density calculations were performed for these samples via the density cup method and the gas pycnometer method, with the results of these calculations used in conjunction with the resin burn-off method to calculate the fiber volume fraction of the fiber-reinforced samples. 3-point bending tests were performed for both the 1k carbon fiber tow-reinforced PLA samples and the pure PLA samples, with the 1k carbon fiber tow-reinforced PLA samples exhibiting 219% the fracture stress of the pure PLA samples and an increase in elastic modulus from 1.795 GPa to 5.871 GPa when compared to the pure PLA samples. 3-point bending test samples were also fabricated of 3k continuous carbon fiber-reinforced PLA plastic, with visually higher quality than the 1k continuous carbon fiber-reinforced PLA samples. Furthermore, small 1-layer, 3-layer and 5-layer laminates were printed of pure PLA plastic and 3k continuous carbon fiber-reinforced PLA plastic for proof of consistent layer height throughout the thickness of the

prints. Unfortunately, thickness measurements were not taken of these laminates due to the campus closure because of the coronavirus.

Future work on this project would begin with finishing the printing of the small 1-layer, 3-layer and 5-layer laminates and measuring them to verify consistent layer height throughout the thickness of the laminate. One would then print large 3-layer or 5-layer laminates and cut samples from those laminates in which the print path is oriented either longitudinally or transversely. The longitudinal and transverse modulus values would be obtained through testing of these samples, and one could then predict theoretical modulus values for samples with any fiber/PLA orientation. This would allow one to compare theoretical modulus with experimentally obtained modulus for future samples printed.

The next step in the future work would be to fabricate and test 3-point bending test samples with 3k carbon fiber tow-reinforced PLA and with pure PLA printed using the parameters of the 3k carbon fiber tow-reinforced PLA samples. The material properties of the 3k carbon fiber tow that is currently stored in the lab are known, and thus the results of testing of samples printed with this tow could be easily compared to other data available through literature. If 1k continuous carbon fiber tow could be obtained of which the material properties are known, then another step in the future work of this project would be to fabricate and test more 1k continuous carbon fiber tow-reinforced PLA samples.

Other future work in this project would be to optimize the fiber coating process. This would include characterizing the effect of the mass fraction of PLA in the PLA/chloroform coating mixture. This would also include potentially designing and fabricating a more robust apparatus for coating the fiber. This system could automate the process of pulling the fiber from one spool, down

through the mixture of PLA and chloroform, past a heat source for drying and back onto another spool.

Future work in this project would also include increasing the fiber volume fraction of the samples. This will come from further optimization of the various parameters of the printing process such as print speed, extrusion multiplier, and hatch spacing. Although the effects of extrusion temperature and layer height were already studied in this project, they could be further studied in the future, as the results of the characterization of these parameters in this project were not entirely telling. Further verification of fiber volume fraction, as well as the study of surface finish and print quality, could be carried out in the future through use of SEM imaging. Other future work could include fabrication and testing of tensile test specimens.

Since the continuous fiber composite 3D printer reported in this thesis is fully developed in-house, the printer can be further modified by integrating real-time damage detection and quality assurance components. Currently, commercial 3D printers rarely incorporate any components for damage and imperfection detection. 3D printers have only been able to include IR cameras and optical cameras in a limited fashion, using IR and optical images to provide a rough estimation of the quality of 3D printed materials and parts [71]. Advanced nondestructive sensors, such as ultrasonic sensors, can be installed in the 3D printer developed in this thesis. Novel nondestructive evaluation and structural health monitoring tools and algorithms, such as time-frequency signal processing and machine learning, can be used to generate 3D imaging to represent microstructures within 3D printed materials [72-78]. In addition, pulsed lasers and even pulsed X-rays can be used to generate high-frequency ultrasounds in 3D printed samples during this printing process, leading to novel real-time monitoring and quality assurance functionalities that can be broadly used in other additive manufacturing systems [79-82].

References

1. Wang, X., et al., *3D printing of polymer matrix composites: A review and prospective.* Composites Part B: Engineering, 2017. **110**: p. 442-458.
2. Ngo, T.D., et al., *Additive manufacturing (3D printing): A review of materials, methods, applications and challenges.* Composites Part B: Engineering, 2018. **143**: p. 172-196.
3. Fard, M.Y., A. Chattopadhyay, and Y. Liu, *Nonlinear 3PB and 4PB flexural behavior and softening localization for epoxy resin E 863 using digital image correlation technique.* Experimental Techniques, 2016. **40**(1): p. 159-171.
4. Fard, M.Y., Y. Liu, and A. Chattopadhyay, *Characterization of epoxy resin including strain rate effects using digital image correlation system.* Journal of Aerospace Engineering, 2012. **25**(2): p. 308-319.
5. Mohan, N., et al., *A review on composite materials and process parameters optimisation for the fused deposition modelling process.* Virtual and Physical Prototyping, 2017. **12**(1): p. 47-59.
6. Malhotra, S.K., K. Goda, and M.S. Sreekala, *Part one introduction to polymer composites.* Polymer Composites, 2012. **1**: p. 1-2.
7. Rohit, K. and S. Dixit, *A review-future aspect of natural fiber reinforced composite.* Polymers from Renewable Resources, 2016. **7**(2): p. 43-59.
8. Prashanth, S., et al., *Fiber reinforced composites-a review.* Journal of Material Sciences & Engineering, 2017. **6**(3): p. 1-6.
9. Hasan, Z., A. Chattopadhyay, and Y. Liu, *An investigation into the performance of composite hat stringers incorporating nanocomposites using a multiscale framework.* Journal of Reinforced Plastics and Composites, 2014. **33**(15): p. 1375-1387.

10. Hasan, Z., A. Chattopadhyay, and Y. Liu, *Multiscale approach to analysis of composite joints incorporating nanocomposites.* Journal of Aircraft, 2015. **52**(1): p. 204-215.

11. Li, N., Y. Li, and S. Liu, *Rapid prototyping of continuous carbon fiber reinforced polylactic acid composites by 3D printing.* Journal of Materials Processing Technology, 2016. **238**: p. 218-225.

12. Ivey, M., et al., *Characterizing short-fiber-reinforced composites produced using additive manufacturing.* Advanced Manufacturing: Polymer & Composites Science, 2017. **3**(3): p. 81-91.

13. Yang, C., et al., *3D printing for continuous fiber reinforced thermoplastic composites: mechanism and performance.* Rapid Prototyping Journal, 2017.

14. Abshirini, M., et al., *Functional nanocomposites for 3D printing of stretchable and wearable sensors.* Applied Nanoscience, 2019. **9**(8): p. 2071-2083.

15. Chavez, L.A., et al., *Fabrication and characterization of 3D printing induced orthotropic functional ceramics.* Smart Materials and Structures, 2019. **28**(12): p. 125007.

16. Chavez, L.A., et al., *Electrical and mechanical tuning of 3D printed photopolymer–MWCNT nanocomposites through in situ dispersion.* Journal of Applied Polymer Science, 2019. **136**(22): p. 47600.

17. Ge, Q., et al., *Active origami by 4D printing.* Smart Materials and Structures, 2014. **23**(9): p. 094007.

18. Cooperstein, I., M. Layani, and S. Magdassi, *3D printing of porous structures by UV-curable O/W emulsion for fabrication of conductive objects.* Journal of Materials Chemistry C, 2015. **3**(9): p. 2040-2044.

19. Postiglione, G., et al., *Conductive 3D microstructures by direct 3D printing of polymer/carbon nanotube nanocomposites via liquid deposition modeling.* Composites Part A: Applied Science and Manufacturing, 2015. **76**: p. 110-114.

20. Popescu, D., et al., *FDM process parameters influence over the mechanical properties of polymer specimens: A review.* Polymer Testing, 2018. **69**: p. 157-166.

21. Alvarez, C., et al., *Investigating the influence of infill percentage on the mechanical properties of fused deposition modelled ABS parts.* Ingeniería e Investigación, 2016. **36**(3): p. 110-116.

22. Wang, J., et al., *Synthesis and characterization of self-assembled ZnO nanoarrays on hybrid structural fibers.* Surfaces and Interfaces, 2019. **16**: p. 188-193.

23. Wang, J., et al., *Development of shape memory polymer nanocomposite foam for treatment of intracranial aneurysms.* Materials Letters, 2019. **250**: p. 38-41.

24. Wang, J., et al., *Shape memory polyurethane with porous architectures for potential applications in intracranial aneurysm treatment.* Polymers, 2019. **11**(4): p. 631.

25. Wang, J., et al., *Synthesis of ZnO nanoarrays on carbon fibers using combined atomic layer deposition and hydrothermal methods.* Materials Research Express, 2018. **5**(6): p. 065029.

26. Chowdhury, S., et al., *Poly dimethylsiloxane/carbon nanofiber nanocomposites: fabrication and characterization of electrical and thermal properties.* International Journal of Smart and Nano Materials, 2016. **7**(4): p. 236-247.

27. Weng, B., et al., *Growth process optimization of ZnO thin film using atomic layer deposition.* Materials Research Express, 2016. **3**(12): p. 126402.

28. ZOU, J., et al., *Self-sensing of Matrix Damage using Mechanophore-based Smart Polymer in Fiber Reinforced Composites.* Journal of Multifunctional Composites, 2014. **2**: p. 207-215.

29. Charara, M., et al., *Highly sensitive compression sensors using three-dimensional printed polydimethylsiloxane/carbon nanotube nanocomposites.* Journal of Intelligent Material Systems and Structures, 2019. **30**(8): p. 1216-1224.

30. Abshirini, M., et al., *3D printing of highly stretchable strain sensors based on carbon nanotube nanocomposites.* Advanced Engineering Materials, 2018. **20**(10): p. 1800425.

31. Frazier, W.E., *Metal additive manufacturing: a review.* Journal of Materials Engineering and Performance, 2014. **23**(6): p. 1917-1928.

32. Huang, S.H., et al., *Additive manufacturing and its societal impact: a literature review.* The International Journal of Advanced Manufacturing Technology, 2013. **67**(5-8): p. 1191-1203.

33. Chowdhury, S.A., et al., *Highly conductive polydimethylsiloxane/carbon nanofiber composites for flexible sensor applications.* Advanced Materials Technologies, 2019. **4**(1): p. 1800398.

34. Charara, M., et al., *Investigation of lightweight and flexible carbon nanofiber/poly dimethylsiloxane nanocomposite sponge for piezoresistive sensor application.* Advanced Engineering Materials, 2019. **21**(5): p. 1801068.

35. Luo, W., et al., *Fabrication and characterization of porous CNF/PDMS nanocomposites for sensing applications.* Applied Nanoscience, 2019. **9**(6): p. 1309-1317.

36. Herren, B., M.C. Saha, and Y. Liu, *Carbon Nanotube-Based Piezoresistive Sensors Fabricated by Microwave Irradiation.* Advanced Engineering Materials, 2019: p. 1901068.

37. Herren, B., et al., *Rapid Microwave Polymerization of Porous Nanocomposites with Piezoresistive Sensing Function.* Nanomaterials, 2020. **10**(2): p. 233.

38. Herren, B., et al., *Enhanced Electrical Conductivity of Carbon Nanotube-Based Elastomer Nanocomposites Prepared by Microwave Curing.* Polymers, 2019. **11**(7): p. 1212.

39. Yan, X., et al., *Lowly loaded carbon nanotubes induced high electrical conductivity and giant magnetoresistance in ethylene/1-octene copolymers.* Polymer, 2016. **103**: p. 315-327.

40. Tang, Y.-S., et al., *Reinforced cyanate ester resins with carbon nanotubes: surface modification, reaction activity and mechanical properties analyses.* Polymer-Plastics Technology and Engineering, 2009. **48**(4): p. 359-366.

41. Chen, H., et al., *Mechanically strong, electrically conductive, and biocompatible graphene paper.* Advanced Materials, 2008. **20**(18): p. 3557-3561.

42. Gu, J., et al., *High thermal conductivity graphite nanoplatelet/UHMWPE nanocomposites.* Rsc Advances, 2015. **5**(46): p. 36334-36339.

43. Gu, J., et al., *Ideal dielectric thermally conductive bismaleimide nanocomposites filled with polyhedral oligomeric silsesquioxane functionalized nanosized boron nitride.* RSC advances, 2016. **6**(42): p. 35809-35814.

44. Perez, A.R.T., D.A. Roberson, and R.B. Wicker, *Fracture surface analysis of 3D-printed tensile specimens of novel ABS-based materials.* Journal of Failure Analysis and Prevention, 2014. **14**(3): p. 343-353.

45. Zhang, J., et al., *3D-printed magnetic Fe 3 O 4/MBG/PCL composite scaffolds with multifunctionality of bone regeneration, local anticancer drug delivery and hyperthermia.* Journal of Materials Chemistry B, 2014. **2**(43): p. 7583-7595.

46. Chung, H. and S. Das, *Processing and properties of glass bead particulate-filled functionally graded Nylon-11 composites produced by selective laser sintering.* Materials Science and Engineering: A, 2006. **437**(2): p. 226-234.

47. Hwang, S., et al., *Thermo-mechanical characterization of metal/polymer composite filaments and printing parameter study for fused deposition modeling in the 3D printing process.* Journal of Electronic Materials, 2015. **44**(3): p. 771-777.

48. Kalsoom, U., et al., *A 3D printable diamond polymer composite: a novel material for fabrication of low cost thermally conducting devices.* RSC advances, 2016. **6**(44): p. 38140-38147.

49. Zhong, W., et al., *Short fiber reinforced composites for fused deposition modeling.* Materials Science and Engineering: A, 2001. **301**(2): p. 125-130.

50. Tekinalp, H.L., et al., *Highly oriented carbon fiber–polymer composites via additive manufacturing.* Composites Science and Technology, 2014. **105**: p. 144-150.

51. Compton, B.G. and J.A. Lewis, *3D Printing: 3D-Printing of Lightweight Cellular Composites (Adv. Mater. 34/2014).* Advanced Materials, 2014. **26**(34): p. 6043-6043.

52. Bakarich, S.E., et al., *Three-dimensional printing fiber reinforced hydrogel composites.* ACS applied materials & interfaces, 2014. **6**(18): p. 15998-16006.

53. Baumann, F., J. Scholz, and J. Fleischer, *Investigation of a new approach for additively manufactured continuous fiber-reinforced polymers.* Procedia Cirp, 2017. **66**: p. 323-328.

54. Hu, Q., et al., *Manufacturing and 3D printing of continuous carbon fiber prepreg filament.* Journal of materials science, 2018. **53**(3): p. 1887-1898.

55. Matsuzaki, R., et al., *Three-dimensional printing of continuous-fiber composites by in-nozzle impregnation.* Scientific reports, 2016. **6**: p. 23058.

56. *Haddington Dynamics*. [cited 2020 March 26]; Available from: https://markforged.com/case-studies/7-axis-robotic-arm/.

57. *Creality3D CR-10 3D Printer*. [cited 2020 March 26]; Available from: https://creality3d.shop/collections/3d-printer/products/creality-cr-10-3d-printer-prusa-i3-diy-kit-aluminum-large-print-size-300x300x400mm.

58. [cited 2020 March 28]; Available from: https://www.walmart.com/ip/DC-12V-360W-30A-Universal-Regulated-Switching-Mode-Power-Supply-for-Creality-3D-Printer-CR-10-CR-10S/273121738?wmlspartner=wlpa&selectedSellerId=101001360&adid=22222222227320863719&wl0=&wl1=g&wl2=c&wl3=399087002541&wl4=pla-865578575434&wl5=9027946&wl6=&wl7=&wl8=&wl9=pla&wl10=128133340&wl11=online&wl12=273121738&veh=sem&gclid=EAIaIQobChMIve3Hs6C-6AIVE8ZkCh1uAQmGEAQYCCABEgJvh_D_BwE.

59. *Generic 3D Printer Kit Mega 2560 + RAMPS 1.4 + 5X A4988 for Arduino RepRap*. [cited 2020 March 28]; Available from: https://yaoota.com/en-ke/product/generic-3d-printer-kit-mega-2560-ramps-14-5x-a4988-for-ardui-price-from-jumia-kenya.

60. *HICTOP Heated Bed Power Module MOSFET Board for Creality CR-10 CR-10S 3D Printer*. [cited 2020 March 29]; Available from: https://www.amazon.com.au/HICTOP-Heated-Module-Creality-Printer/dp/B07MTG6G8J.

61. *Creality 3D® 12864 LCD Display Screen For Ender-3 3D Printer*. [cited 2020 March 29]; Available from: https://www.banggood.com/Creality-3D-12864-LCD-Display-Screen-For-Ender-3-3D-Printer-p-1350131.html?cur_warehouse=CN.

62. Cojuhari, I., et al. *Automatic temperature control in 3D printing of the polymer details*. in *2017 International Conference on Electromechanical and Power Systems (SIELMEN)*. 2017. IEEE.

63. Tian, X., et al., *Recycling and remanufacturing of 3D printed continuous carbon fiber reinforced PLA composites.* Journal of cleaner production, 2017. **142**: p. 1609-1618.

64. Tian, X., et al., *Interface and performance of 3D printed continuous carbon fiber reinforced PLA composites.* Composites Part A: Applied Science and Manufacturing, 2016. **88**: p. 198-205.

65. Woern, A.L., et al., *Fused particle fabrication 3-D printing: Recycled materials' optimization and mechanical properties.* Materials, 2018. **11**(8): p. 1413.

66. Emiliano, S. *All About the Density of PLA*. 2019 [cited 2020 April 11]; Available from: https://all3dp.com/2/pla-density-what-s-the-density-of-pla-filament-plastic/.

67. MInus, M. and S. Kumar, *The processing, properties, and structure of carbon fibers.* Jom, 2005. **57**(2): p. 52-58.

68. Gibson, R.F., *principles of composite material mechanics 2nd Ed*. 2007, Taylor & Francis.

69. Fu, S.-Y., B. Lauke, and Y. Mai, *Science and engineering of short fibre reinforced polymers composites. 2009*. Cambridge, UK Woodhead Publishing.

70. *Standard Test Methods for Flexural Properties of Unreinforced and Reinforced Plastics and Electrical Insulating Materials*. 2014, ASTM International.

71. Wu, P., J. Wang, and X. Wang, *A critical review of the use of 3-D printing in the construction industry.* Automation in Construction, 2016. **68**: p. 21-31.

72. Liu, Y., et al., *Damage assessment of CFRP composites using a time–frequency approach.* Journal of Intelligent Material Systems and Structures, 2012. **23**(4): p. 397-413.

73. Liu, Y. and S. Nayak, *Structural health monitoring: State of the art and perspectives.* Jom, 2012. **64**(7): p. 789-792.

74. Liu, Y., et al., *Application of system-identification techniquest to health monitoring of on-orbit satellite boom structures.* Journal of Spacecraft and Rockets, 2011. **48**(4): p. 589-598.

75. Liu, Y., S. Mohanty, and A. Chattopadhyay, *Condition based structural health monitoring and prognosis of composite structures under uniaxial and biaxial loading.* Journal of Nondestructive Evaluation, 2010. **29**(3): p. 181-188.

76. Liu, Y. and A. Chattopadhyay, *Low-velocity impact damage monitoring of a sandwich composite wing.* Journal of Intelligent Material Systems and Structures, 2013. **24**(17): p. 2074-2083.

77. Ou, J. and H. Li, *Structural health monitoring in mainland China: review and future trends.* Structural health monitoring, 2010. **9**(3): p. 219-231.

78. Mitra, M. and S. Gopalakrishnan, *Guided wave based structural health monitoring: A review.* Smart Materials and Structures, 2016. **25**(5): p. 053001.

79. Wang, S., et al., *Ultrahigh Resolution Pulsed Laser-Induced Photoacoustic Detection of Multi-Scale Damage in CFRP Composites.* Applied Sciences, 2020. **10**(6): p. 2106.

80. Wang, S., et al. *Non-Destructive Evaluation of Composite and Metallic Structures using Photo-Acoustic Method*. in *AIAA Scitech 2019 Forum*. 2019.

81. Wang, S., et al. *Photo-Acoustic Based Non-Contact and Non-Destructive Evaluation for Detection of Damage Precursors in Composites*. in *ASME 2018 International Mechanical Engineering Congress and Exposition*. 2018. American Society of Mechanical Engineers Digital Collection.

82. Tang, S., et al., *X-ray-induced acoustic computed tomography of concrete infrastructure.* Applied Physics Letters, 2018. **112**(6): p. 063504.